TABLE 1. Sequences of primers used in real-time PCR analyses and 3'UTR cloning for luciferase reporter assay

Gene	Accession no.	Sequence
Real-time PCR		
CDK2	NM_001798	Forward: 5'-CTCCACCGAGACCTTAAACCTCAG-3' Reverse: 5'-TCGGTACCACAGGGTCACCA-3'
CDK4	NM_000075	Forward: 5'-GATAGATGCTGACCCATACCTCAAG-3' Reverse: 5'-ATGCTGTGGTGCTTTGAGGTAG-3
CDK6	NM_001259	Forward: 5'-ATATCTGCCTACAGTGCCCTGTCTC-3' Reverse: 5'-GTGGGAATCCAGGTTTTCTTTGCAC-3'
Cyclin E1	NM_001238	Forward: 5'-GCAGTATCCCCAGCAAATC-3' Reverse: 5'-TCAAGGCAGTCAACATCCA-3'
Cyclin D1	NM_053056	Forward: 5'-GCTGTGCATCTACACCGACAACTC-3' Reverse: 5'-AGGTTCCACTTGAGCTTGTTCACC-3'
E2F3	NM_001949	Forward: 5'-CCAACTCAGGACATAGCGATTGCTC-3' Reverse: 5'-AGGAATTTGGTCCTCAGTCTGCTGT-3'
GAPDH	NM_002046	Forward: 5'-GCACCGTCAAGGCTGAGAAC-3' Reverse: 5'-TGGTGAAGACGCCAGTGGA-3'
p21	NM_000389	Forward: 5'-AGCAGAGGAAGACCATGTGGA-3' Reverse: 5'-GGAGTGGTAGAAATCTGTCATGCT-3'
p27	NM_004064	Forward: 5'-AGCTTGCCCGAGTTCTACTACAG-3' Reverse: 5'-ACCAAATGCGTGTCCTCAGAGT-3'
3'UTR cloning		
Cyclin E1	NM_001238	Forward: 5'-TTCTCGAGATCCTTCTCCACCAAAGACAGTT-3' Reverse: 5'-TTTCTAGAGAATGGATAGATATAGCAGCACTTACA-3'

The forward and reverse primers for 3'UTR cloning carried the *Xho*I and *Xba*I sites at their 5'-ends, respectively.

HSCs. Because miR-195 is categorized into the same family as miR-15b and miR-16 and has been reported to regulate cell cycle by targeting E2F3, CDK6, and cyclin D1 (Xu et al., 2009), we suspect the involvement of miR-195 in the proliferation of HSC and in type I IFN, in particular IFN-β, -induced inhibition of their growth.

Materials and Methods

Materials

Human HSC line LX-2 was donated by Dr. Scott L. Friedman (Mount Sinai School of Medicine, New York, NY) (Xu et al., 2005). Necessary reagents and materials were obtained from the

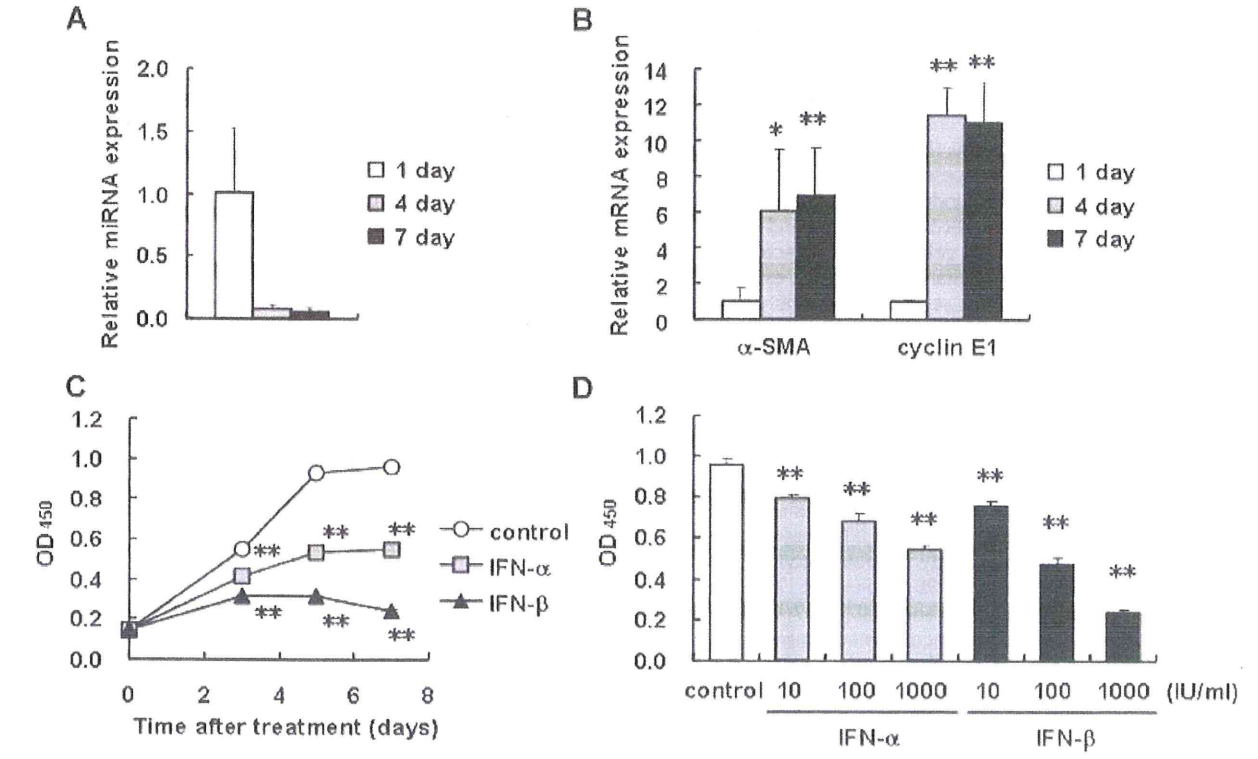

Fig. 1. Expression of miR-195 in mouse HSCs during primary culture and growth inhibitory effect of IFN-α and -β on human stellate cells. A,B: Isolated mouse HSCs were cultured for the indicated periods. The expression levels of miR-195 (A), and α-SMA and cyclin E1 mRNA (B) were measured by real-time PCR. *$P < 0.05$, **$P < 0.01$ compared with 1 day. C,D: LX-2 cells were incubated with IFN-α or -β (1,000 IU/ml) for 3–7 days (C), or with IFN-α or -β at the concentration of 10–1,000 IU/ml for 7 days (D). Control indicates non-treated cells. The proportion of viable cells was determined using a WST-1 assay. **$P < 0.01$ compared with control.

following sources: Dulbecco's modified Eagle's medium (DMEM) from Sigma Chemical Co. (St. Louis, MO); fetal bovine serum (FBS) from Invitrogen (Carlsbad, CA); human natural IFN-α and -β from Otsuka Pharmaceutical Co. (Tokushima, Japan) and Toray Industries, Inc. (Tokyo, Japan), respectively; precursor and inhibitor of miR-195, and the corresponding negative controls from Ambion (Austin, TX); mouse monoclonal antibody against cyclin E1, cyclin D1 and p21, and glyceraldehyde-3-phosphate dehydrogenase (GAPDH) from MBL (Nagoya, Japan), Cell Signaling Technology, Inc. (Beverly, MA), and Chemicon International, Inc. (Temecula, CA), respectively; rabbit polyclonal antibodies against cyclin-dependent kinase (CDK) 6 and E2F3 from Santa Cruz Biotechnology, Inc. (Santa Cruz, CA); goat polyclonal antibody against CDK4 from Santa Cruz Biotechnology, Inc.; enhanced Chemiluminescence plus detection reagent from GE Healthcare (Buckinghamshire, UK); Immobilon P membranes from Millipore Corp. (Bedford, MA); reagents for cDNA synthesis and real-time PCR from Toyobo (Osaka, Japan); a cell counting kit from Dojindo Laboratories (Kumamoto, Japan); and all other reagents from Sigma Chemical Co. or Wako Pure Chemical Co. (Osaka, Japan).

Cells

LX-2 cells were maintained in DMEM supplemented with 10% FBS (DMEM/FBS) and were plated at a density of 0.7–1.5 × 10^4 cells/cm^2 24 h prior to biological assay. Biological assays were done in DMEM/FBS unless stated otherwise. Mouse primary HSCs were isolated from male C57BL/6 mice by the pronase-collagenase digestion method as described previously (Uyama et al., 2006) and were cultured in DMEM/FBS.

Transient transfection of miRNA precursors and inhibitors

Precursor of miR-195, which was a double-strand RNA mimicking endogenous miR-195 precursor, and the negative control with a scrambled sequence were transfected into LX-2 cells using Lipofectamine 2000 (Invitrogen) at a final concentration of 50 nM in accordance with the manufacturer's instructions. Briefly, miRNA precursor and Lipofectamine 2000 were mixed at a ratio of 25 (pmol):1 (μl) in Opti-MEM I Reduced Medium (Invitrogen), incubated for 20 min at room temperature, and were then added to the cultures. After 24 h, the culture medium was replaced with fresh medium. Inhibitor of miR-195, which was designed to bind to endogenous miR-195 and inhibit its activity, and the negative control with a scrambled sequence were transfected similarly. After 6 h, the culture medium was changed and IFN-β was added successively.

Cell proliferation assay

LX-2 cells were plated at a density of 2 × 10^3 cells/well in 96-well plates 24 h prior to experiments. The culture medium was replaced by fresh medium containing different concentrations of IFNs at days 0 and 3. After 3, 5, and 7 days of treatment, cell proliferation was measured by WST-1 assay. In another experiment, the cells

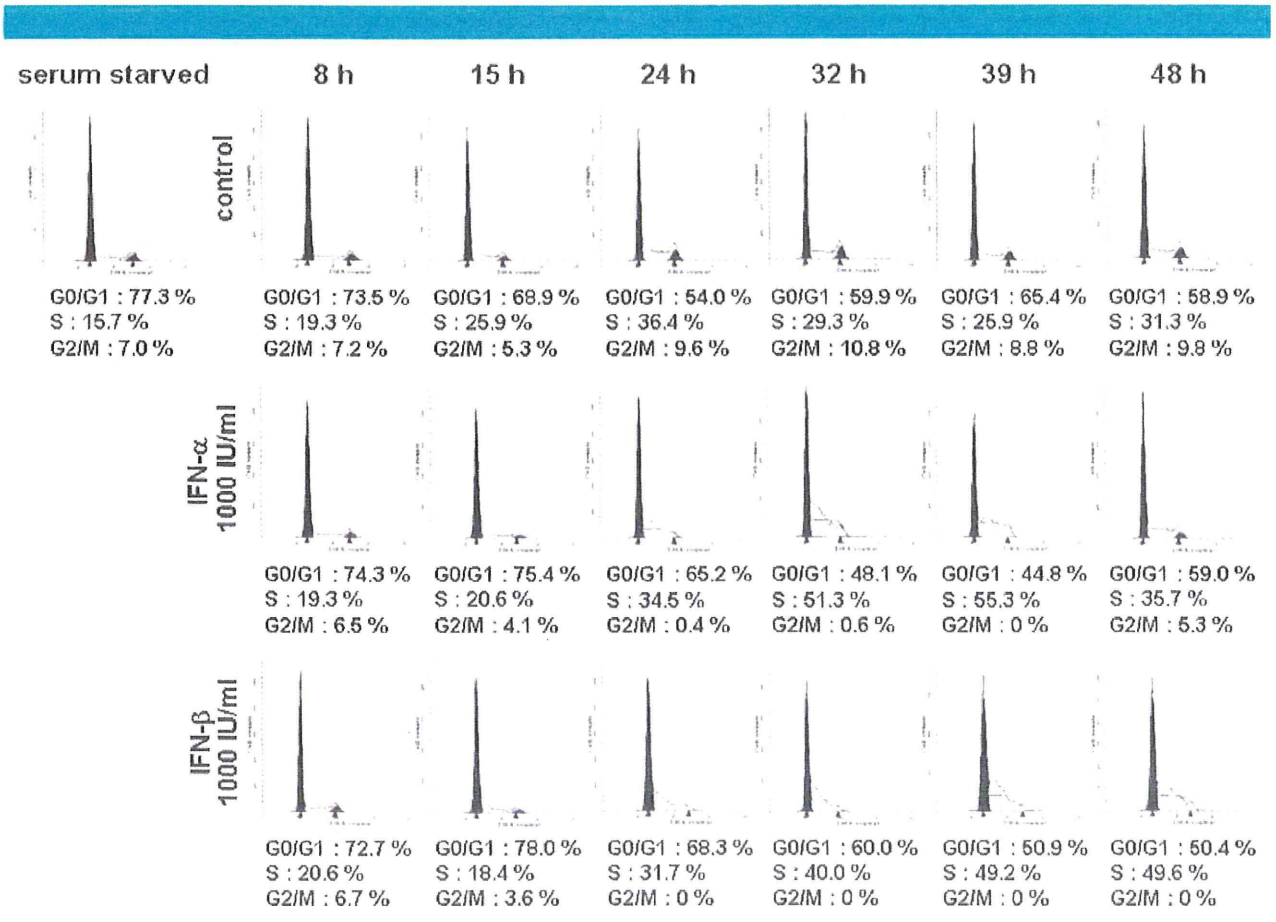

Fig. 2. Effect of IFN-α and -β on cell cycle distribution in human stellate cells. LX-2 cells synchronized in G0/G1 phase were then incubated with IFN-α or -β (1,000 IU/ml) in DMEM/FBS for the indicated periods. Control indicates non-treated cells. The cell cycle was analyzed by flow cytometry. The white, black, and shaded region indicates the histogram measured by flow cytometry, G0/G1 phase (left) or G2/M phase (right), and S phase, respectively, as analyzed by ModFIT LT software.

were plated at a density of 3×10^3 cells/well in 96-well plate for 24 h prior and were then transfected with the miR-195 precursor as described above. After 24 h, the medium was changed and the culture was continued for an additional 1–3 days before the measurement of cell proliferation.

Cell cycle analysis

Cells were serum starved for 24 h and then the medium was replaced with IFN-containing DMEM/FBS. At the indicated time points after treatment, the cells were harvested by trypsinization, washed in phosphate-buffered saline (PBS), and fixed in ice-cold 70% ethanol. The cells were washed in PBS and resuspended in PBS containing 500 μg/ml RNase A and incubated for 20 min. Cellular DNA was stained with propidium iodide at a final concentration of 25 μg/ml for 20 min. The cells were analyzed using a FACSCalibur HG flow cytometer (Becton Dickinson, Franklin Lakes, NJ). A total of 20,000 events were counted for each sample. Data were analyzed using ModFIT LT software (Verity Software House, Topsham, ME).

Quantitative real-time PCR

Quantitative real-time PCR was performed according to the method described elsewhere with use of a set of gene-specific oligonucleotide primers (Table 1) using an Applied Biosystems Prism 7500 (Applied Biosystems, Foster City, CA) (Ogawa et al., 2010). To detect miR-195 expression, the reverse transcription reaction was performed using a TaqMan microRNA Assay (Applied Biosystems) in accordance with the manufacturer's instructions. The expression level of GAPDH was used to normalize the relative abundance of mRNAs and miR-195.

Immunoblotting

Cells were lysed in RIPA buffer [50 mM Tris/HCl, pH 7.5, 150 mM NaCl, 1% NP-40, 0.5% sodium deoxycholate, 0.1% sodium dodecyl sulfate (SDS)] containing Protease Inhibitor Cocktail, Phosphatase Inhibitors Cocktail 1, and Phosphatase Inhibitor Cocktail 2 (Sigma). Proteins (20 μg) were electrophoresed in a 10% SDS–polyacrylamide gel and then transferred onto Immobilon P membranes (Ogawa et al., 2010). Immunoreactive bands were visualized by the enhanced chemiluminescence system using a Fujifilm Image Reader LAS-3000 (Fuji Medical Systems, Stamford, CT).

Luciferase reporter assay

Interaction of miR-195 to the 3′UTR of the cyclin E1 gene was tested according to the reported method (Ogawa et al., 2010). The 3′UTR of the cyclin E1 gene containing putative miR-195 target regions was obtained by PCR using cDNA derived from LX-2 and a primer set listed in Table 1. The obtained DNA fragments (497 bp) were inserted into a pmirGLO Vector (Promega, San Luis Obispo,

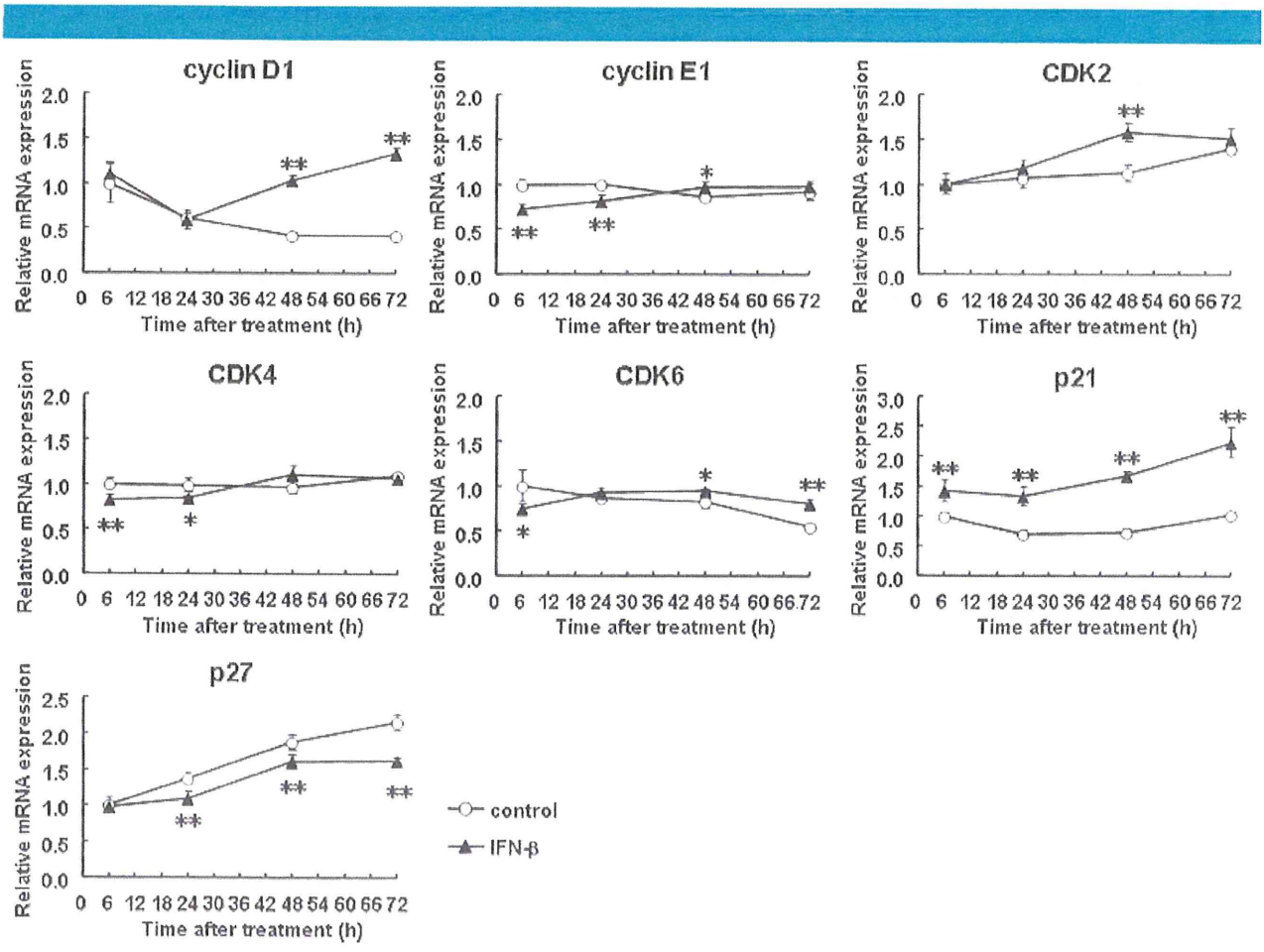

Fig. 3. Expression of cell cycle-related genes in stellate cells. LX-2 cells were incubated with IFN-β (1,000 IU/ml) for up to 72 h for determining the expression levels of mRNAs of cyclin D1, cyclin E1, CDK2, CDK4, CDK6, p21, and p27. Control indicates non-treated cells. *$P < 0.05$, **$P < 0.01$ compared with control.

CA). LX-2 cells, plated in 96-well plates at a density of 2×10^4 cells/well 24 h prior to experiment, were transfected with 200 ng of reporter plasmid and miRNA precursor using Lipofectamine 2000. After 24 h, the medium was changed to 20 μl of PBS. The Dual-Glo Luciferase Assay System (Promega) was used to analyze luciferase expression in accordance with the manufacturer's protocol. Firefly luciferase activity was normalized to *Renilla* luciferase activity to adjust for variations in transfection efficiency among experiments.

Statistical analysis

Data presented as graphs are the means ± SD of at least three independent experiments. Statistical analysis was performed using Student's *t*-test. $P < 0.05$ was considered significant.

Results

Reduction of miR-195 expression during activation of primary-cultured HSCs

It has been known that, when maintained in a plastic culture plate, freshly isolated primary-cultured HSCs undergo spontaneous activation and transformation into myofibroblastic cells that express α-SMA and produce fibrogenic mediators, such as type I collagen and transforming growth factor-β. In our preliminary experiments using primary-cultured mouse HSCs, we noticed that the cells drastically decreased the expression of miR-195 when they underwent spontaneous activation (unpublished observation). The present study confirmed this notion as shown in Figure 1A. miR-195 expression level certainly decreased in activation process of primary-cultured mouse HSCs. In contrast, the expression levels of α-SMA and cyclin E1 mRNA increased (Fig. 1B). Accordingly, we considered that miR-195 plays a role as an antiproliferative and antiactivating miRNA in HSCs. As a matter of fact, there was a study showing that miR-16 family including miR-195 inhibits proliferation of lung cancer cells by silencing cyclins D1 and E1, and CDK6 (Liu et al., 2008). The result indicated by Figure 1 and the cited study together drove us to explore the IFN's antiproliferative action on HSCs (Mallat et al., 1995; Shen et al., 2002), focusing on miR-195 and cell cycle-related genes.

Effects of IFN-α and -β on proliferation of HSCs

First, we investigated the effects of type I IFNs on the proliferation of LX-2 cells using a WST-1 assay. LX-2 cells in control culture continued to grow during the experimental

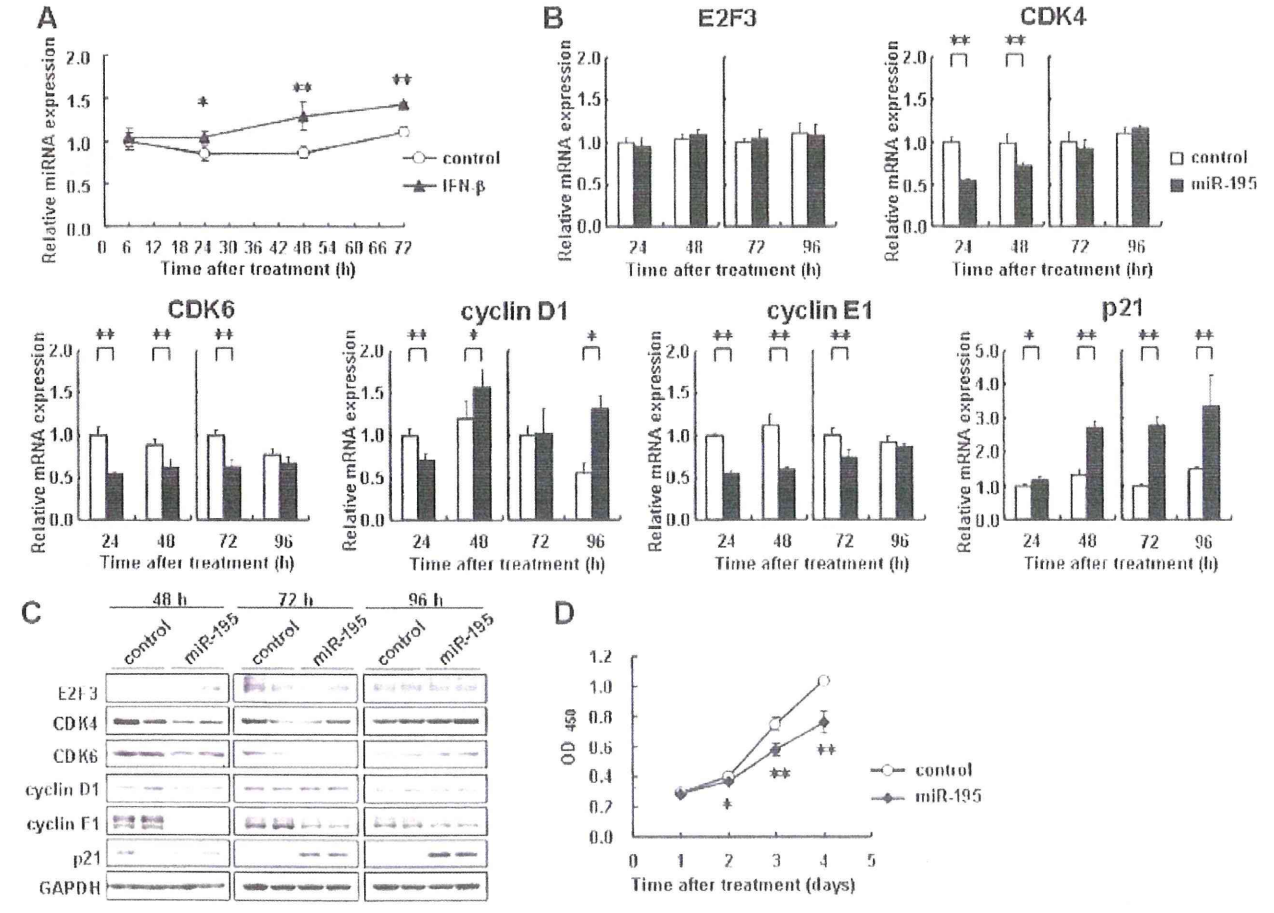

Fig. 4. Regulation of expression of cell cycle regulators by miR-195. A: LX-2 cells were incubated with IFN-β (1,000 IU/ml) for up to 72 h for determining the expression levels of miR-195. Control indicates non-treated cells. *$P < 0.05$, **$P < 0.01$ compared with control. B–D: LX-2 cells were transfected with 50 nM miR-195 precursor or a negative control (control). B: mRNA expression levels of E2F3, CDK4, CDK6, cyclin D1, cyclin E1, and p21 measured at 24, 48, 72, and 96 h post-transfection. C: Protein expression of E2F3, CDK4, CDK6, cyclin D1, cyclin E1, and p21 examined at 48, 72, and 96 h post-transfection. D: Growth of LX-2 cells transfected with 50 nM miR-195 precursor or a negative control (control) was measured using a WST-1 assay. *$P < 0.05$, **$P < 0.01$ compared with control.

period of 7 days (Fig. 1C). IFN-α and -β both, but the latter more actively, decreased cell proliferation time-dependently at a concentration of 1,000 IU/ml, supporting the previous studies (Mallat et al., 1995; Shen et al., 2002). Dose-dependency of the growth inhibition is shown in IFN concentrations from 10 to 1,000 IU/ml (Fig. 1D).

Effects of IFN-α and -β on cell cycle distribution

To elucidate the mechanism of the growth inhibitory effect of IFN, we next examined the change in cell cycle distribution in response to IFN-α and -β treatment by flow cytometry. LX-2 cells were synchronized in G0/G1 phase by serum starvation for 24 h. In non-treated cells (control), population in G0/G1 phase was reduced after serum exposure, which was accompanied by the increase of population in S phase. This cell cycle transition peaked at 24 h (Fig. 2, upper part). In cells treated with IFN-α or -β, the G0/G1 phase population was larger and the S phase population was smaller than in the control cells at 15 h and 24 h. In addition, the accumulation of cells in early S phase was observed at 32–48 h (Fig. 2, middle and lower parts). These delays in cell cycle shift were more potent in IFN-β-treated cells than in IFN-α-treated cells. It was concluded that type I IFN hampered HSC proliferation through a delay in the cell cycle at the transition from G1 to S phase and in the progression of S phase.

Regulation of cyclin E1 and p21 expression by IFN-β

IFN-β was chosen in the following experiments because of its more potent inhibition of cell cycle progression than IFN-α as described above. The transition from G1 to S phase and the progression of S phase are known to be influenced by various regulators (Golias et al., 2004). Among them, we found that IFN-β significantly decreased cyclin E1 mRNA expression levels by 0.6- to 0.7-fold at 6 and 24 h and increased p21 mRNA expression levels by 1.4- to 2.3-fold at 6, 24, 48, and 72 h in LX-2 cells (Fig. 3). The expression levels of CDK4 and CDK6 were also reduced by IFN-β at early phase with less extent. The others showed negligible change within 24 h although variable dynamics were seen thereafter; changes of cyclin D1, CDK2, and p27 expression at late phase were toward cell cycle promotion with currently unknown reason.

Regulation of miR-195 expression by IFN-β

The result indicated from Figure 1 strongly suggested the possibility that IFN-β increase the expression of miR-195 in LX-2 cells. To test this possibility, we examined the expression levels of miR-195 in IFN-β-treated LX-2 cells. As a result, the miR-195 expression level was significantly increased by IFN-β treatment at 24, 48, and 72 h (Fig. 4A).

Regulation of cyclin E1 and p21 expression by miR-195

The results obtained from experiments shown in Figures 3 and 4A led us to hypothesize that IFN-β up-regulates the expression of miR-195, which then down-regulates the expression of cyclin E1 and up-regulates the expression of p21. In addition, there had been a study reporting that miR-195 targets E2F3, CDK6, and cyclin D1 in addition to cyclin E1 (Xu et al., 2009). Under these considerations, we examined the changes in the expression levels of the above-mentioned cell cycle-related molecules and CDK4 by introducing miR-195

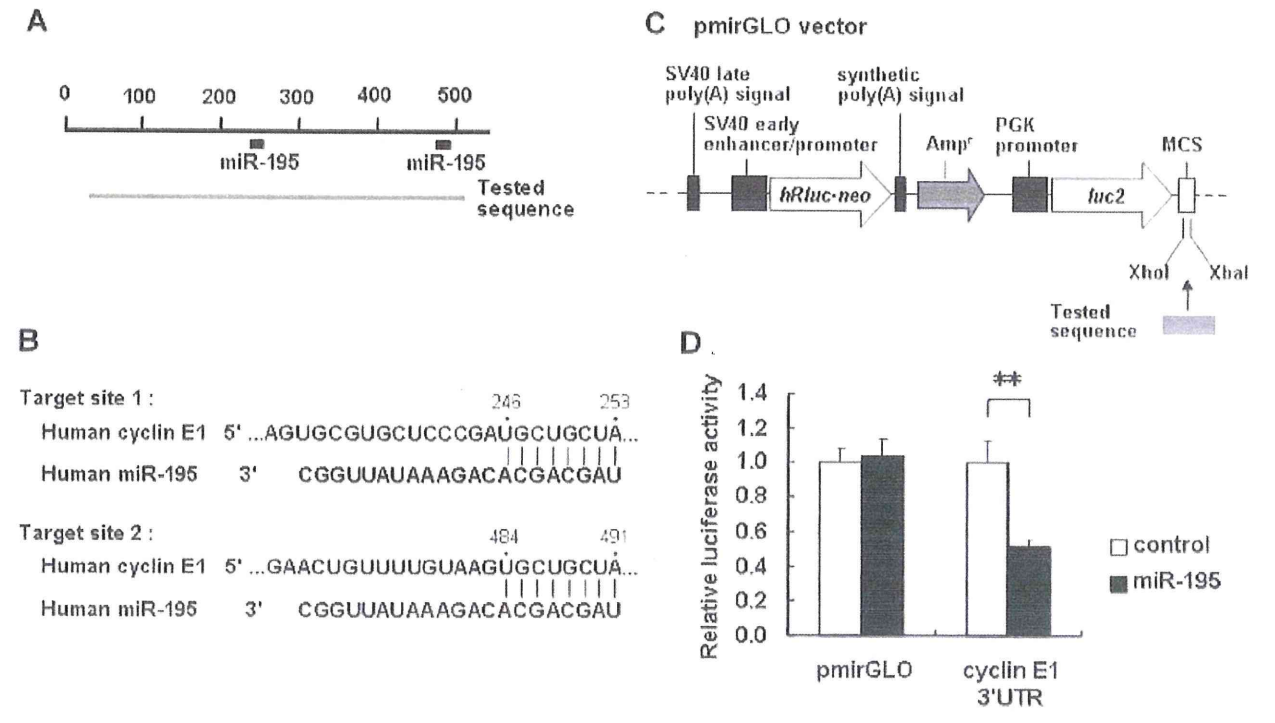

Fig. 5. Interaction of miR-195 with the 3′UTR of cyclin E1 mRNA. A: Schematic indication of the putative miR-195 target sites in the 3′UTR of the cyclin E1 mRNA. Tested sequences indicate the regions that were inserted into the luciferase reporter vector. B: Predicted pairing of the target region and miRNAs. C: Structure of the luciferase reporter vector (Ogawa et al., 2010). The putative miR-195 target region in cyclin E1 3′UTR (tested sequence) was ligated into the MCS. Arrows indicate the gene directions. Amp^R indicates an ampicillin resistance gene. D: Reporter gene assay of the interaction between the 3′UTR of cyclin E1 mRNA and miR-195 in LX-2 cells. Results are expressed as the relative activities against the activity in the presence of the control. $^*P < 0.05$, $^{**}P < 0.01$ compared with control.

precursor into LX-2 cells. Transfection of miR-195 precursor increased the miR-195 expression levels in LX-2 cells by up to 10,000–30,000 times compared with those in cells transfected with negative control (data not shown). Cyclin E1 mRNA and protein expression levels showed a remarkable reduction up to 72 h as result of miR-195 overexpression (Fig. 4B,C). On the other hand, p21 mRNA and protein expression levels showed a marked increase. CDK4, CDK6, and cyclin D1 expression levels were significantly changed at the mRNA level, but negligibly at the protein level. E2F3 mRNA and protein expression levels were unchanged (Fig. 4B,C). These results suggested that miR-195 mainly regulated cyclin E1 and p21 expression in LX-2 cells. Moreover, transfection of miR-195 precursor (50 nM) decreased the proliferation of LX-2 cells in the WST-1 assay (Fig. 4D). These results showed that miR-195 down-regulates endogenous cyclin E1 expression and up-regulates p21 expression, resulting in the attenuation of cell cycle progression and cell proliferation.

Interaction of miR-195 with cyclin E1 3′UTR in LX-2 cells

Next, we examined whether miR-195 interacted directly with cyclin E1 3′UTR in LX-2 cells. The predicted miRNA target sites for miR-195 in the cyclin E1 3′UTR were analyzed using TargetScan Human Release 5.1 (http://www.targetscan.org/). The cyclin E1 3′UTR contained two target sites for miR-195 (Fig. 5A,B). To investigate the direct interaction between them, the part of the cyclin E1 3′UTR containing the two miR-195 target sites (497 bp) was cloned from LX-2 cells, inserted the downstream of a firefly luciferase reporter gene in a pmirGLO vector (Fig. 5C), and cotransfected into LX-2 cells. As shown in Figure 5D, luciferase reporter activity decreased significantly in miR-195 precursor-transfected cells compared with cells transfected with a negative control of the precursor. These results suggested a direct interaction between miR-195 and cyclin E1 3′UTR in LX-2 cells. Binding site of miR-195 was not found in p21 3′UTR by TargetScan.

Regulation of cyclin E1 expression by IFN-β and miR-195

To confirm the contribution of miR-195 to the inhibitory effect of IFN-β on cyclin E1 expression, LX-2 cells were first transfected with 50 nM miR-195 inhibitor and then treated with 1,000 IU/ml IFN-β. As shown in Figure 6A, miR-195 inhibitor blocked the inhibitory effect of IFN-β on cyclin E1 mRNA expression at 16 and 24 h. Although there was no difference in the cyclin E1 mRNA expression between IFN-β-treated cells and non-treated cells (control) at 48 h, the cyclin E1 mRNA expression level in miR-195 inhibitor plus IFN-β-treated cells was up-regulated compared with non-treated cells (Fig. 6A). Immunoblot analysis revealed that miR-195 inhibitor elevated the cyclin E1 expression level of IFN-β-treated cells at 24 and 48 h (Fig. 6B).

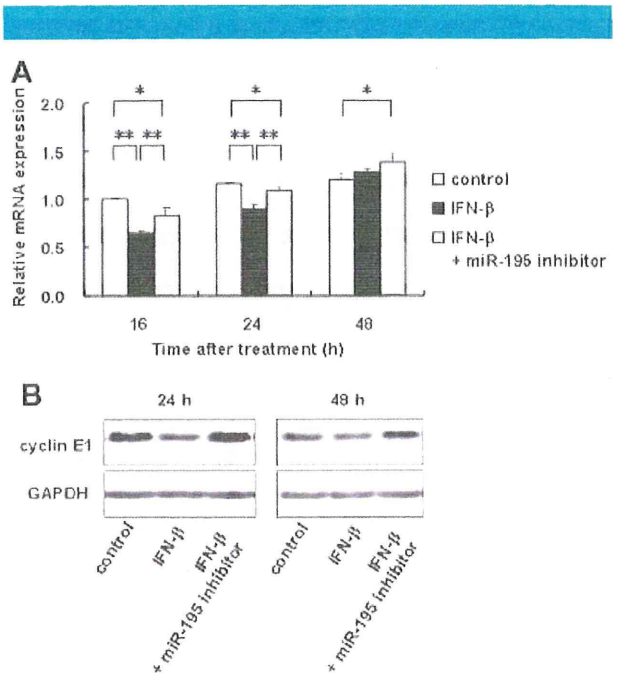

Fig. 6. Regulation of cyclin E1 expression by IFN-β and miR-195. LX-2 cells were transfected with 50 nM miR-195 inhibitor or a negative control. After 6 h, the culture medium was changed and then IFN-β (1,000 IU/ml) was added. Cells were then incubated for the indicated time periods. A: mRNA expression levels of cyclin E1. B: Protein expression levels of cyclin E1. GAPDH are for loading adjustment. Control; cells were transfected with a negative control and incubated without IFN-β. *$P < 0.05$, **$P < 0.01$.

Discussion

In this study, we showed that IFN-β is more antiproliferative on LX-2 cells than IFN-α, which appears to be contradictory to their known mechanism of action: both IFN-α and -β exert their activities through the common signaling pathway, beginning with binding to the same type I IFN receptor (IFNAR) consisting of IFNAR1 and IFNAR2, which activate the common components of janus kinase/signal transducer and activator of transcription (STAT) pathway (Darnell et al., 1994). However, a similar activity difference between the IFNs has also been demonstrated in colon cancer cell lines (Katayama et al., 2007) and in rat HSCs (Shen et al., 2002). Some studies showed that IFN-β but not IFN-α formed a stable complex with IFNARs, suggesting that IFN-β may interact with IFNAR chains in a manner different from IFN-α (Croze et al., 1996; Russell-Harde et al., 1999).

We showed here that IFN-β down-regulated the expression of cyclin E1 and up-regulated the expression of p21, which caused the cells to be less active proceeding in the transition from G0 to G1 phase and in the progression of S phase. The cell cycle is regulated by various molecules, such as cyclins and CDKs. Cyclin E is essential in activating CDK2. The cyclin E-CDK2 complex phosphorylates pRb at G1 phase, leading to gene transcription activities that are needed in S phase, and also activates the factors involved in DNA replication at early S phase (Golias et al., 2004). It has been reported that cyclin E1 expression increased in non-parenchymal cells of human fibrotic liver and that cyclin E1-deficient mice developed milder liver fibrosis compared with wild-type mice after CCl_4 administration (Nevzorova et al., 2010). These results imply that cyclin E1 regulates the progression of liver fibrosis by accelerating HSC proliferation.

The most frequent miRNAs that targets cyclin E1 are the miR-16 family, which consists of miR-15, -16, -195, -424, and -497 (Liu et al., 2008; Wang et al., 2009). We here observed the induction of miR-195 by IFN-β. miR-195 was reported to be down-regulated in human HCC tissues and to suppress HCC growth through the targeted interference of cyclin D1, CDK6, and E2F3 in a *xenograft* mouse model (Xu et al., 2009), while it was reported to target cyclin E1 in addition to the above-mentioned factors in A549 cells (Liu et al., 2008). miR-15b and miR-16 are down-regulated concomitantly with HSC activation and their overexpression induces apoptosis and a delay of cell cycle in HSCs by targeting Bcl-2 and cyclin D1 (Guo et al., 2009a,b). However, the role of miR-195 in HSCs remains unknown. We showed here that miR-195 expression was

decreased during spontaneous activation of primary-cultured mouse HSCs and that miR-195 interacted with cyclin E1 3′UTR and lowered the expression levels of the cyclin E1 mRNA and protein in LX-2 cells. These results suggest that the down-regulation of miR-195 may associate with the proliferation of HSCs in fibrotic liver similarly to miR-15 and miR-16. In this study, the changes of the protein expression levels of E2F3, CDK6, and cyclin D1, which were reported to be regulated by miR-195 (Xu et al., 2009), were negligible by miR-195, although the exact reason for this phenomenon was not determined. However, because the total context scores obtained by TargetScan were −0.73 for cyclin E1, −0.33 for E2F3, −0.32 for cyclin D1, and −0.09 for CDK6, the result obtained here was thought to be reasonable. In addition, minimal or negligible effect of miR-195 on the expression of E2F3, CDK4, CDK6, and cyclin D1 was compatible with that of IFN-β on these factors. Furthermore, inhibition of miR-195 by miR-195 inhibitor attenuated the effect of IFN-β on cyclin E1 expression, though not so strong. Taken together, it is most likely that the down-regulation of cyclin E1 by IFN-β treatment in HSCs is mediated through miR-195 up-regulation. The mechanism through which IFN-β induces miR-195 in LX-2 cells need to be explored further.

It is well known that IFNs induce the expression of p21 in various cancer cells (Sangfelt et al., 1999; Katayama et al., 2007). We also observed the up-regulation of p21 in IFN-β-treated cells. Therefore, p21, in addition to cyclin E1, may play a role in IFN-induced growth inhibition of HSCs. Until now, it has been reported that IFNs induce p21 expression through the binding of STAT and IFN regulatory factor, which are critical signaling molecules after IFN-IFNAR interaction, to p21 gene promoter (Gartel and Tyner, 1999). Unexpectedly, we found the up-regulation of p21 by miR-195 (Fig. 4). The results obtained here raise a new possibility that the up-regulation of p21 by IFN-β in HSCs may be partially mediated through miR-195.

In conclusion, type I IFN, in particular IFN-β, inhibited the proliferation of human HSCs by delaying the cell cycle in G1 to early S phase through the down-regulation of cyclin E1 and up-regulation of p21. The cyclin E1 down-regulation and p21 up-regulation were partially mediated by miR-195 that was up-regulated by IFN-β. This study raises a new mechanistic aspect of the antifibrotic effect of IFN in liver fibrosis and the possibility of influencing miR-195 as a therapeutic strategy for liver fibrosis.

Acknowledgments

This work was supported by a grant from the Ministry of Health, Labour and Welfare of Japan to N. Kawada (2008–2010).

Literature Cited

Bartel DP. 2004. MicroRNAs: Genomics, biogenesis, mechanism, and function. Cell 116:281–297.

Bataller R, Brenner DA. 2001. Hepatic stellate cells as a target for the treatment of liver fibrosis. Semin Liv Dis 21:437–451.

Chang XM, Chang Y, Jia A. 2005. Effects of interferon-alpha on expression of hepatic stellate cell and transforming growth factor-beta1 and alpha-smooth muscle actin in rats with hepatic fibrosis. World J Gastroenterol 11:2634–2636.

Croze E, Russell-Harde D, Wagner TC, Pu H, Pfeffer LM, Perez HD. 1996. The human type I interferon receptor. Identification of the interferon beta-specific receptor-associated phosphoprotein. J Biol Chem 271:33165–33168.

Darnell JE, Kerr IM, Stark GR. 1994. Jak-STAT pathways and transcriptional activation in response to IFNs and other extracellular signaling proteins. Science 264:1415–1421.

Fort J, Pilette C, Veal N, Oberti F, Gallois Y, Douay O, Rosenbaum J, Cales P. 1998. Effects of long-term administration of interferon alpha in two models of liver fibrosis in rats. J Hepatol 29:263–270.

Friedman SL. 2000. Molecular regulation of hepatic fibrosis, an integrated cellular response to tissue injury. J Biol Chem 275:2247–2250.

Gartel AL, Tyner AL. 1999. Transcriptional regulation of the p21(WAF1/CIP1) gene. Exp Cell Res 246:280–289.

Golias CH, Charalabopoulos A, Charalabopoulos K. 2004. Cell proliferation and cell cycle control: A mini review. Int J Clin Pract 58:1134–1141.

Guo CJ, Pan Q, Jiang B, Chen GY, Li DG. 2009a. Effects of upregulated expression of microRNA-16 on biological properties of culture-activated hepatic stellate cells. Apoptosis 14:1331–1340.

Guo CJ, Pan Q, Li DG, Sun H, Liu BW. 2009b. miR-15b and miR-16 are implicated in activation of the rat hepatic stellate cell: An essential role for apoptosis. J Hepatol 50:766–778.

Inagaki Y, Nemoto T, Kushida M, Meng Y, Higashi K, Ikeda K, Kawada N, Shirasaki F, Takehara K, Sugiyama K, Fujii M, Yamauchi H, Nakao A, de Crombrugghe B, Watanabe T, Okazaki I. 2003. Interferon alpha down-regulates collagen gene transcription and suppresses experimental hepatic fibrosis in mice. Hepatology 38:890–899.

Ji JF, Shi J, Budhu A, Yu ZP, Forgues M, Roessler S, Ambs S, Chen YD, Meltzer PS, Croce CM, Qin LX, Man K, Lo CM, Lee J, Ng IOL, Fan J, Tang ZY, Sun HC, Wang XW. 2009a. MicroRNA expression, survival, and response to interferon in liver cancer. N Engl J Med 361:1437–1447.

Ji JL, Zhang JS, Huang GC, Qian J, Wang XQ, Mei S. 2009b. Over-expressed microRNA-27a and 27b influence fat accumulation and cell proliferation during rat hepatic stellate cell activation. FEBS Lett 583:759–766.

Katayama T, Nakanishi K, Nishihara H, Kamiyama N, Nakagawa T, Kamiyama T, Iseki K, Tanaka S, Todo S. 2007. Type I interferon prolongs cell cycle progression via p21(WAF1/CIP1) induction in human colon cancer cells. Int J Oncol 31:613–620.

Liu Q, Fu HJ, Sun F, Zhang HM, Tie Y, Zhu J, Xing RY, Sun ZX, Zheng XF. 2008. miR-16 family induces cell cycle arrest by regulating multiple cell cycle genes. Nucleic Acids Res 36:5391–5404.

Mallat A, Preaux AM, Blazejewski S, Rosenbaum J, Dhumeaux D, Mavier P. 1995. Interferon alpha and gamma inhibit proliferation and collagen synthesis of human Ito cells in culture. Hepatology 21:1003–1010.

Nevzorova YA, Bangen JM, Gassler N, Haas U, Weiskirchen R, Tacke F, Sicinski P, Trautwein C, Liedtke C. 2010. Cyclin E1 controls the cell cycle activity of hepatic stellate cells and triggers fibrogenesis in mice. J Hepatol 52:S374–S375.

Ogawa T, Kawada N, Ikeda K. 2009. Effect of natural interferon alpha on proliferation and apoptosis of hepatic stellate cells. Hepatol Int 3:497–503.

Ogawa T, Iizuka M, Sekiya Y, Yoshizato K, Ikeda K, Kawada N. 2010. Suppression of type I collagen production by microRNA-29b in cultured human stellate cells. Biochem Biophys Res Commun 391:316–321.

Pedersen IM, Cheng G, Wieland S, Volinia S, Croce CM, Chisari FV, David M. 2007. Interferon modulation of cellular microRNAs as an antiviral mechanism. Nature 449:919–922.

Pestka S, Langer JA, Zoon KC, Samuel CE. 1987. Interferons and their actions. Annu Rev Biochem 56:727–777.

Russell-Harde D, Wagner TC, Perez HD, Croze E. 1999. Formation of a uniquely stable type I interferon receptor complex by interferon beta is dependent upon particular interactions between interferon beta and its receptor and independent of tyrosine phosphorylation. Biochem Biophys Res Commun 255:539–544.

Sangfelt O, Erickson S, Castro J, Heiden T, Gustafsson A, Einhorn S, Grander D. 1999. Molecular mechanisms underlying interferon-alpha-induced G0/G1 arrest: CKI-mediated regulation of G1 Cdk-complexes and activation of pocket proteins. Oncogene 18:2798–2810.

Shen H, Zhang M, Minuk GY, Gong YW. 2002. Different effects of rat interferon alpha, beta and gamma on rat hepatic stellate cell proliferation and activation. BMC Cell Biol 3:9.

Tanabe J, Izawa A, Takemi N, Miyauchi Y, Torii Y, Tsuchiyama H, Suzuki T, Sone S, Ando K. 2007. Interferon-beta reduces the mouse liver fibrosis induced by repeated administration of concanavalin A via the direct and indirect effects. Immunology 122:562–570.

Uyama N, Zhao L, Van Rossen E, Hirako Y, Reynaert H, Adams DH, Xue Z, Li Z, Robson R, Pekny M, Geerts A. 2006. Hepatic stellate cells express synemin, a protein bridging intermediate filaments to focal adhesions. Gut 55:1276–1289.

Uze G, Schreiber G, Piehler J, Pellegrini S. 2007. The receptor of the type I interferon family. Curr Top Microbiol Immunol 316:71–95.

Venugopal SK, Jiang J, Kim TH, Li Y, Wang SS, Torok NJ, Wu J, Zern MA. 2010. Liver fibrosis causes downregulation of miRNA-150 and miRNA-194 in hepatic stellate cells, and their overexpression causes decreased stellate cell activation. Am J Physiol Gastrointest Liver Physiol 298:G101–G106.

Wang F, Fu XD, Zhou Y, Zhang Y. 2009. Down-regulation of the cyclin E1 oncogene expression by microRNA-16-1 induces cell cycle arrest in human cancer cells. BMB Rep 42:725–730.

Xu L, Hui AY, Albanis E, Arthur MJ, O'Byrne SM, Blaner WS, Mukherjee P, Friedman SL, Eng FJ. 2005. Human hepatic stellate cell lines, LX-1 and LX-2: New tools for analysis of hepatic fibrosis. Gut 54:142–151.

Xu T, Zhu Y, Xiong YJ, Ge YY, Yun JP, Zhuang SM. 2009. MicroRNA-195 suppresses tumorigenicity and regulates G(1)/S transition of human hepatocellular carcinoma cells. Hepatology 50:113–121.

Growth Hormone-Dependent Pathogenesis of Human Hepatic Steatosis in a Novel Mouse Model Bearing a Human Hepatocyte-Repopulated Liver

Chise Tateno, Miho Kataoka, Rie Utoh, Asato Tachibana, Toshiyuki Itamoto, Toshimasa Asahara, Fuyuki Miya, Tatsuhiko Tsunoda, and Katsutoshi Yoshizato

Yoshizato Project (C.T., M.K., R.U., A.T., K.Y.), Hiroshima Prefectural Institute of Industrial Science and Technology, Cooperative Link of Unique Science and Technology for Economy Revitalization (CLUSTER), and PhoenixBio, Co. Ltd. (C.T., A.T., K.Y.), Higashihirosima, Hiroshima 739-0046, Japan; Hiroshima University Liver Project Research Center (C.T., T.A., K.Y.) and Division of Frontier Medical Science (T.I., T.A.), Department of Surgery, and Hiroshima University 21st Century COE Program for Advanced Radiation Casualty Medicine, Programs for Biomedical Research, Graduate School of Biomedical Sciences, Hiroshima University, Hiroshima, Hiroshima 734-8551, Japan; Laboratory for Medical Informatics (F.M., T.T.), Center for Genomic Medicine, RIKEN, Yokohama, Kanagawa 230-0045, Japan; Developmental Biology Laboratory and Hiroshima University 21st Century COE Program for Advanced Radiation Casualty Medicine (K.Y.), Department of Biological Science, Graduate School of Science, Hiroshima University, Higashihiroshima, Hiroshima 739-8526, Japan; and Departments of Hepatology and Liver Research Center (K.Y.), Graduate School of Medicine, Osaka City University, Osaka 545-8586, Japan

Clinical studies have shown a close association between nonalcoholic fatty liver disease and adult-onset GH deficiency, but the relevant molecular mechanisms are still unclear. No mouse model has been suitable to study the etiological relationship of human nonalcoholic fatty liver disease and human adult-onset GH deficiency under conditions similar to the human liver *in vivo*. We generated human (h-)hepatocyte chimeric mice with livers that were predominantly repopulated with h-hepatocytes in a h-GH-deficient state. The chimeric mouse liver was mostly repopulated with h-hepatocytes about 50 d after transplantation and spontaneously became fatty in the h-hepatocyte regions after about 70 d. Infusion of the chimeric mouse with h-GH drastically decreased steatosis, showing the direct cause of h-GH deficiency in the generation of hepatic steatosis. Using microarray profiles aided by real-time quantitative RT-PCR, comparison between h-hepatocytes from h-GH-untreated and -treated mice identified 14 GH-up-regulated and four GH-down-regulated genes, including *IGF-I*, *SOCS2*, *NNMT*, *IGFLS*, *P4AH1*, *SLC16A1*, *SRD5A1*, *FADS1*, and *AKR1B10*, respectively. These GH-up- and -down-regulated genes were expressed in the chimeric mouse liver at lower and higher levels than in human livers, respectively. Treatment of the chimeric mice with h-GH ameliorated their altered expression. h-Hepatocytes were separated from chimeric mouse livers for testing *in vitro* effects of h-GH or h-IGF-I on gene expression, and results showed that GH directly regulated the expression of *IGF-I*, *SOCS2*, *NNMT*, *IGFALS*, *P4AH1*, *FADS1*, and *AKR1B10*. In conclusion, the chimeric mouse is a novel h-GH-deficient animal model for studying *in vivo* h-GH-dependent human liver dysfunctions. **(*Endocrinology* 152: 1479–1491, 2011)**

To study pathophysiological characteristics of the human liver, we previously generated a humanized (chimeric) mouse whose liver was almost completely repopulated with human (h-)hepatocytes by transplanting h-hepatocytes into immunodeficient and liver-damaged mice, which had been obtained by mating an albumin enhancer/promoter-driven

ISSN Print 0013-7227 ISSN Online 1945-7170
Printed in U.S.A.

doi: 10.1210/en.2010-0953 Received August 18, 2010. Accepted January 10, 2011.
First Published Online February 8, 2011

Abbreviations: AGHD, Adult-onset GH deficiency; Alb, albumin; CK, cytokeratin; GO, gene ontology; h-, human; m-, mouse; 9MM, 9-month-old male; NAFLD, nonalcoholic fatty liver disease; NASH, nonalcoholic steatohepatitis; ORO, Oil Red O; qRT-PCR, quantitative RT-PCR; RI, replacement index; SCID, severe combined immunodeficient; uPA, urokinase-type plasminogen-activator; 25YF, 25-yr-old female; 61YF, 61-yr-old female; 28YM, 28-yr-old male; 57YM, 57-yr-old male.

urokinase-type plasminogen-activator (uPA) transgenic mouse with a severe combined immunodeficient (SCID) mouse (uPA/SCID mouse) (1–3). The replacement index (RI), the occupancy ratio of h-hepatocytes to the total [h- and mouse (m-)] hepatocytes in the chimeric mouse liver, indicated the degree of replacement with h-hepatocytes. The RI in the mice was as high as 96% (1). h-Hepatocytes therein expressed mRNA for drug-metabolizing enzymes and transporters as in donor livers (1, 4, 5). However, we noticed that the mice spontaneously developed hepatic steatosis as the time after transplantation was prolonged. The h-hepatocytes of a chimeric mouse are in a GH-deficient state (6) primarily because human cells do not react with rodent GH (7), thus suggesting that the observed lipid accumulation in h-hepatocytes was caused by a lack of available h-GH in chimeric mice.

A concern is increasing about nonalcoholic fatty liver disease (NAFLD) as a significant complication of obesity and as a hepatic manifestation of the metabolic syndrome (8). There are striking similarities between obesity and untreated adult-onset GH deficiency (AGHD), indicating that homeostatic imbalance of GH is an etiological factor of obesity (9). NAFLD is related to hypopituitary and hypothalamic dysfunction (10–12). AGHD is featured as decrease in body mass, increase in visceral adiposity, and abnormal lipid profile (13), which are associated with hepatic steatosis (11, 13, 14). One study showed that reduction in GH concentration was a predictor of NAFLD in adult males (15) and another that GH administration drastically improved the fatty liver of AGHD patients (13, 14). A suitable GH-dependent lipogenetic animal model is currently absent, in which we can investigate the *in vivo* effects of h-GH on h-hepatocytes at the cellular and molecular levels.

In this study, we first tested the hypothesis that h-hepatocytes in chimeric mouse liver develop steatosis due to the lack of circulating h-GH. In fact, hepatic steatosis was induced in the mouse liver but not when the chimeric mice were treated with h-GH. We then compared gene expression profiles between h-GH-treated and -untreated chimeric mouse h-hepatocytes to identify h-GH-regulated lipogenesis genes. Furthermore, we examined whether h-GH directly regulates the expression of lipogenesis-related genes or of h-IGF-I levels using cultured chimeric mouse h-hepatocytes. As a whole, the chimeric mouse was proved to be a suitable animal model for studying the etiological relationship among AGHD, GH, and NAFLD in GH-related aspects of metabolic syndrome.

Materials and Methods

We performed studies under the ethical approval of the Hiroshima Prefectural Institute of Industrial Science and Technology Ethics Board and the Ethics Committee at the Hiroshima University Hospital.

Preparation of h-hepatocytes

Livers were obtained from four donors [a 28-yr-old male (28YM) and a 57-yr-old male (57YM) and a 25-yr-old female (25YF) and a 61-yr-old female (61YF)] after receiving informed consent before surgery, according to the 1975 Declaration of Helsinki. h-Hepatocytes were isolated from the liver tissues as previously reported (1). Real-time quantitative RT-PCR (qRT-PCR) was performed on these human livers and/or on h-hepatocytes isolated from h-liver tissues (Table 1).

Donor cells for chimeric mice were h-hepatocytes from a Caucasian 9-month-old male (9MM) infant and an African-American 6-yr-old girl (6YF) purchased from In Vitro Technologies (Baltimore, MD) and BD Biosciences Discovery Labware (San Jose, CA), respectively.

Animals, transplantation of h-hepatocytes, and treatment of chimeric mice with h-GH

Production of uPA/SCID mice (1) and examination of their zygosity in uPA transgenes (16) were performed as previously reported. Homozygotic mice (20–30 d old) were used as hosts for all transplantation experiments. The 9MM and 6YF hepatocytes (hepatocytes$_{9MM}$ and hepatocytes$_{6YF}$, respectively), 7.5–10.0 $\times$ 10^5 cells per animal, were transplanted into six uPA/SCID mice (Table 2) for microarray and real-time qRT-PCR analysis and into 41 mice [36 mice for steatosis analysis (Fig. 1C) and five mice for steatosis analysis under h-GH treatment (Fig. 2E)], as previously described (1). Chimeric mice were killed 48–118 d after transplantation.

Three chimeric mice with hepatocytes$_{9MM}$ [nos. 4–6 (Table 2)], three chimeric mice with hepatocytes$_{6YF}$ [nos. 4–6 (Table 2)], one chimeric mouse$_{9MM}$ (not included in Table 2), and one chimeric mouse$_{6YF}$ (not included in Table 2) were continuously infused with 2.5 mg/kg·d h-GH (Wako, Osaka, Japan) through an sc-implanted Alzet micro-osmotic pump (Alza Corp., Palo Alto, CA) for 2 wk before killing (6, 17). Blood h-albumin (Alb) and serum h-IGF-I in the mice were quantified as previously reported (6).

Immunohistochemistry, lipid staining, and grading of steatosis in h-hepatocytes of chimeric mouse liver

Formalin-fixed paraffin sections from the left lateral lobe of six chimeric mice$_{6YF}$ were stained with mouse anti-h-cytokeratin (CK) 18 monoclonal antibodies (clone CD10; Dako Cytomation, Glostrup, Denmark) that did not react m-hepatocytes as

TABLE 1. Human liver tissues used in real-time qRT-PCR

Objectives	Age (yr)	Sex	RT-PCR
25YF	25	F	Cell and tissue
28YM	28	M	Cell and tissue
57YM	57	M	Cell
61YF	61	F	Cell and tissue

F, Female; M, male.

TABLE 2. Chimeric mice used in microarray analysis and real-time qRT-PCR

Donors	Animal number (sex)	Treatment with h-GH[a]	Days after transplantation	h-Alb in blood (mg/ml)	h-IGF-I in sera (ng/ml)	RI_{Alb} (%)[b] or RI_{immuno} (%)[c]	Microarray or RT-PCR
9MM	1 (F)	–	72	16.1	ND	>95[b]	Cell
	2 (F)	–	75	10.4	ND	>95[b]	
	3 (F)	–	101	6.0	ND	80[b]	
	4 (M)	+	75	8.1	ND	95[b]	
	5 (F)	+	75	6.2	ND	80[b]	
	6 (F)	+	75	5.9	ND	80[b]	
6YF	1 (F)	–	97	3.5	<9.4	75.1[c]	Tissue
	2 (F)	–	90	6.5	<9.4	78.1[c]	
	3 (F)	–	111	5.2	<9.4	70.2[c]	
	4 (M)	+	84	5.3	69.6	85.3[c]	
	5 (F)	+	84	3.7	64.8	70.3[c]	
	6 (F)	+	84	5.9	83.0	81.5[c]	

F, Female; M, male; ND, not determined.

[a] –, untreated with h-GH; +, treated with hGH.

[b] RI calculated by the blood h-Alb levels using the formula of the correlation curve $y = 0.0006x^2 + 0.0281x - 0.0042$ ($r^2 = 0.60$) in which x and y represent RI and blood h-Alb level, respectively.

[c] RI determined by immunohistological staining of liver sections.

previously described (18). The area occupied by h-CK18-positive (h-CK18$^+$) hepatocytes was identified to calculate RI (1).

Frozen sections were prepared from the livers of five h-GH-treated and 36 chimeric h-GH-untreated $mice_{6YF}$ and stained with Oil Red O (ORO). When necessary, serial sections were stained with anti-h-CK8/18 antibodies (MP Biomedicals, Aurora, OH) that did not react with m-hepatocytes as previously described (19). Steatosis grading of h-hepatocytes was performed on ORO-stained chimeric mouse liver sections as follows: grade 0, no lipid droplets; grade 1, appearance of small lipid droplets; grade 2, small and middle-sized lipid droplets; grade 3, small to large droplets (Fig. 1B).

Isolation of h-hepatocytes from chimeric mouse livers for gene expression profiles

Livers were isolated 72–101 d after transplantation from h-GH-untreated control chimeric $mice_{9MM}$ [nos. 1–3 (Table 2)] and h-GH-treated chimeric $mice_{9MM}$ [nos. 4–6 (Table 2)]. These livers were disaggregated by two-step collagenase perfusion as previously described (20), except perfusion was for 20 min and centrifugation was three times 2 min at 50 × *g*. Pelleted hepatocytes (h-$hepatocytes_{chimeric\ mouse}$) were treated with RLT buffer solution in an RNeasy Mini kit (QIAGEN K.K., Tokyo, Japan) and stored in a deep freezer until RNA isolation for microarray and real-time qRT-PCR.

Purity of h-hepatocytes$_{chimeric\ mouse}$

We previously established the correlation curve for chimeric $mice_{9MM}$ between the blood h-Alb concentration and RI_{immuno}, which is determined immunohistologically from liver tissue sections (1). The correlation curve predicted that chimeric $mice_{9MM}$ for microarray and real-time qRT-PCR examinations had a RI_{Alb} higher than 80% (Table 2). Apparently, this RI was a lower estimation of the real h-hepatocyte purity in hepatocyte preparations because m-hepatocytes were often lost during collagenase digestion due to fragility against the enzyme. Thus, the correct h-hepatocyte purity in the $hepatocytes_{chimeric\ mouse/9MM}$ (hepatocytes isolated from chimeric mouse liver bearing h-$hepatocytes_{9MM}$) was determined as follows. Among chimeric $mice_{6YF}$, we selected 10 mice whose RI_{Alb} at the time of death was similar to that of the chimeric $mice_{9MM}$ and isolated h-$hepatocytes_{chimeric\ mouse}$ from them. They were incubated with K8216 antibodies that react with the cell surface of h- but not m-hepatocytes (21) and then with secondary antibody, followed by fluorescence-activated cell sorting analysis to determine the percentage of h-hepatocytes in the $hepatocytes_{chimeric\ mouse}$. The h-hepatocyte purity was 90.8 ± 6.4% (n = 10). The presence of m-hepatocytes in $hepatocytes_{chimeric\ mouse}$ at less than 10% did not affect microarray assays as described in *Results*.

Microarray analysis

RNAs were extracted using TRIzol reagent (Invitrogen, Carlsbad, CA) from h-hepatocytes and h-liver tissues isolated from h-GH-untreated and -treated chimeric mice and were used for microarray analysis at the hepatocyte and liver tissue levels, respectively (Table 2). The array profiles were compared between h-GH-treated and -untreated samples, and statistical significance tests were performed. We deposited our array data to NCBI GEO (Gene Expression Omnibus, http://www.ncbi.nlm.nih.gov/geo/query/acc.cgi?acc=GSE26224, GEO ID GSE26224).

Microarray at the hepatocyte level

Six chimeric $mice_{9MM}$ [nos. 1–6 (Table 2)] were used in the hepatocyte level microarray assay. Half of the chimeric mice (nos. 1–3) were as h-GH-untreated control animals and the remaining half (nos. 4–6) as h-GH-treated animals by treating with h-GH during the last 2 wk before killing. h-$Hepatocytes_{chimeric\ mouse}$ were isolated from h-GH-untreated and -treated chimeric $mice_{9MM}$ at 72–101 d and 75 d after transplantation, respectively, for total RNA isolation.

The RNA samples were treated with deoxyribonuclease (QIAGEN K.K.), purified using ribonuclease-free deoxyribonuclease set (QIAGEN K.K.) and RNeasy Mini Kit (QIAGEN K.K.), and applied to an Affymetrix GeneChip Human Genome U133 Plus 2.0 Array (Affymetrix, Santa Clara, CA) that had been spotted with 54,675 human transcripts. Microarray data were normalized using GCOS software version 1.3 (Affymetrix). The

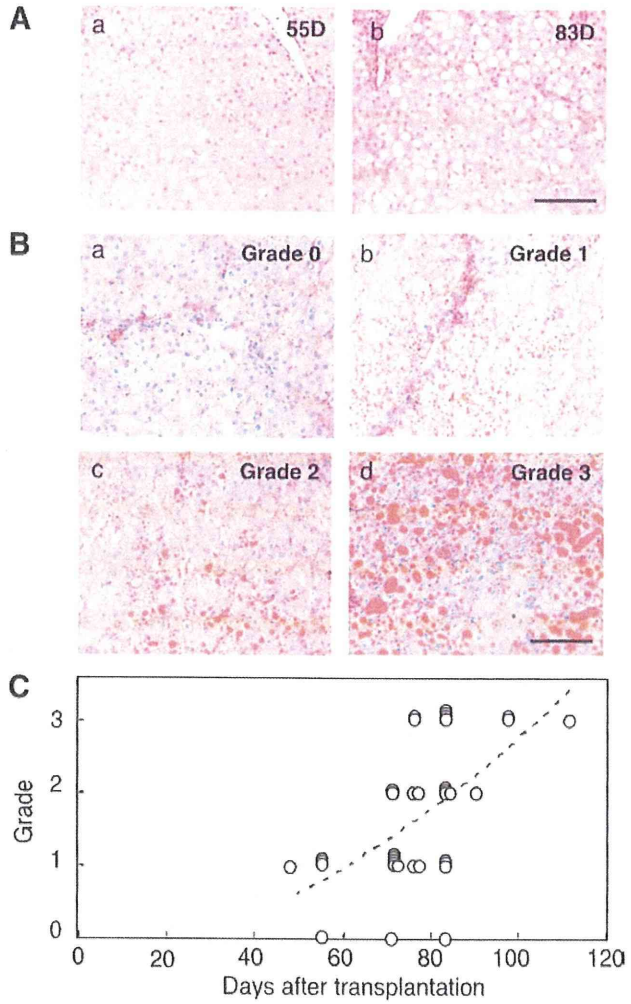

FIG. 1. Lipid accumulation in chimeric mouse h-hepatocytes. Chimeric mice$_{6YF}$ were killed 48–111 d after transplantation for histological examinations by hematoxylin and eosin (A) and ORO liver staining (B). A, h-Hepatocyte regions in the mice killed at 55 d (55D) (a) and 83 d (83D) (b). No visible cytoplasmic vacuolation in the h-hepatocytes at 55 d, but extensive and intensive vacuolation at 83 d. B, Grading of steatosis. Photos of typical staining show various levels of lipid accumulation with nuclei stained *blue*. Lipid accumulation was graded as described in the text: a, grade 0 (55 d); b, grade 1 (77 d); c, grade 2 (83 d); d, grade 3 (97 d). *Bars*, 100 μm. C, Relationship between steatosis grade and duration (days) after transplantation. The steatosis grade increased according to the following relationship: $y = 0.0002x^2 + 0.0102x - 0.4416$, where x is days after transplantation, and y is steatosis grade. The correlation coefficient was $r^2 = 0.3455$. The *dashed line* represents the best-fit curve for the above equation.

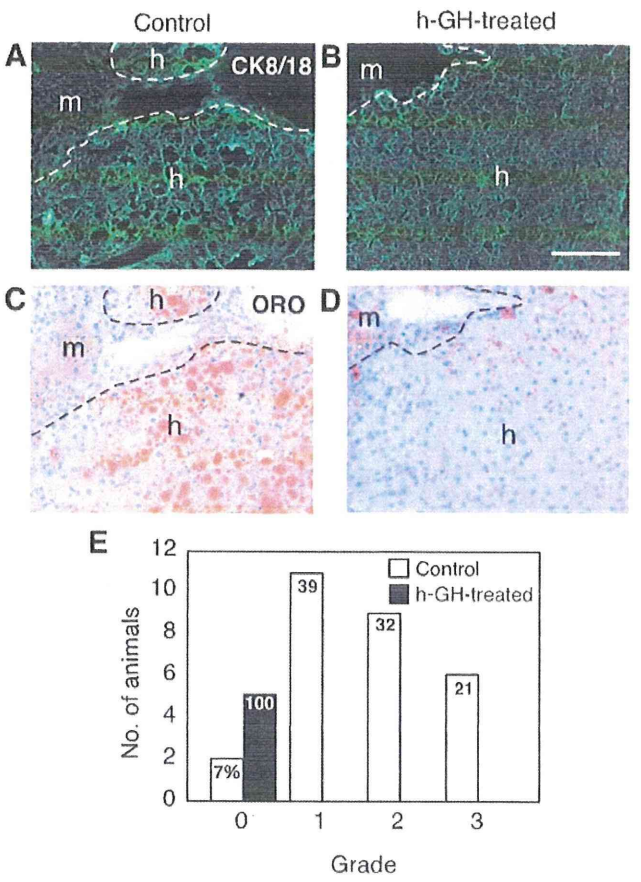

FIG. 2. Effects of h-GH on liver steatosis. Five chimeric mice$_{6YF}$ were given h-GH in the last 2 wk before being killed 70–90 d after transplantation. Twenty-eight of the mice$_{6YF}$ shown in Fig. 1C were killed at 70–90 d as h-GH-untreated animals. A–D, Histology. A control (6YF, no. 1 in Table 2) (A) and h-GH-treated mouse (6YF no. 4 in Table 2] (B) were killed at 97 and 84 d after h-hepatocyte transplantation, respectively, for h-CK8/18 immunohistochemistry to identify h-hepatocytes. Primary antibodies were visualized with Alexa 594-conjugated anti-m-IgG goat sera (Molecular Probes, Eugene, OR). Serial sections from the control (C) and h-GH-treated mouse (D) were stained with ORO. Small to large droplets are diffusely distributed in h-hepatocytes from control chimeric liver (grade 3) but are absent in h-GH-treated animals (grade 0); m and h indicate regions of m- and h-hepatocytes, respectively. *Dotted lines* show the boundary between the two regions. *Bar*, 100 μm. E, Steatosis graded for 28 controls (*white bars*) and five h-GH-treated chimeric mice (*black bar*). *Arabic numerals* in the *bars* represent the percentage in each case (control or h-GH-treated animals). All h-GH-treated chimeric mice were of grade 0.

obtained mRNA expression profiles were referred to as profiles at the hepatocyte level: profiles of h-GH-untreated (n = 3) and h-GH-treated h-hepatocytes$_{\text{chimeric mouse}}$ (n = 3).

Microarray analysis at the liver tissue level

Six chimeric mice$_{6YF}$ [nos. 1–6 (Table 2)] were used for the liver tissue-level assay. Half of six chimeric mice$_{6YF}$ (nos. 4–6) were treated with h-GH, and the other half (nos. 1–3) served as controls. Liver tissues consisted of three visually identifiable regions of different colors. White, red, and medium-colored regions between the white and red regions corresponded to those of original diseased m-hepatocytes, uPA gene-deleted m-hepatocytes, and h-hepatocytes, respectively (1). h-Hepatocyte regions were dissected from livers of chimeric mice$_{6YF}$ using a razor blade for RNA extraction. The obtained mRNA expression profiles were referred to as profiles at the liver tissue level.

Determination of gene expression by real-time qRT-PCR

mRNA expression was determined by real time qRT-PCR in human livers and h-GH-untreated and -treated chimeric mouse livers for h-GH-regulated genes selected from microarray analysis and lipogenesis-related genes (Table 3). Sources for extraction of total RNA are shown in Tables 1 and 2. cDNA was

TABLE 3. Primers

Gene	Forward primers (5′–3′)	Reverse primers (5′–3′)
IGF-I	GCTTCCGGAGCTGTGATCTAA	GCTGACTTGGCAGGCTTG
SOCS2	GCAAGGATAAGCGGACAGG	GCGGTTTGGTCAGATAAAGGT
NNMT	CCGGGAGGCAGTAGAGGC	GTCCTTCGTTGTTGGCCAT
IGFLS	TCTGCAGGGCGAAGTCC	
KLOTHO	AGCCATTATACCACCATCCTTG	GTCGGTCATTTCTTGCACTTCTA
P4AH1	TGGATACCCATTTGTTGCCA	
SLC16A1	TGCTGGAGCCCTCATGC	TTCCAGCTTTCTCAAGGGATG
SRD5A1	TACGTATTCAAATAAGCCTCCCCT	
SCD	TCAAAACAGTGTGTTCGTTGC	CATAAGGACGATATCCGAAGAGG
FADS1	CAGGCCACATGCAATGTC	ATCTAGCCAGAGCTGCCCTG
FADS2	GGCTCTCCAGGAACCTGATG	
FASN	GGCAAATTCGACCTTTCTCAG	AGGACCCCGTGGAATGTC
DGAT2	ACGGCCTTACCTGGCTACA	AGACATCAGGTACTCCCTCAACAC
ADPN	CCTCCAGGTCCCAAATGCC	CCAGTCCTGCTCAGGTGTGC
AKR1B10	GGCCTGTAACGTGTTGC	ATGGGACATGAGTGGAGG
SREBP1c	CATGGATTGCACATTTGAAG	CAGAGAGGAGGCCAGAGAA
FABP	GATCCAAAACGAATTCACGG	ATTGTCACCTTCCAACTGAACC
GAPDH	CCACCTTTGACGACGCTGGG	CATACCAGGAAATGAGCTTGACA

synthesized using 1 μg RNA and PowerScript reverse transcriptase (Clontech, Mountain View, CA) and oligo-deoxythymidine primers (Invitrogen) and was subjected to real-time qRT-PCR following the manufacturer's instructions. Genes were amplified with a set of gene-specific primers (Table 3) and SYBR Green PCR mix in a PRISM 7700 sequence detector (Applied Biosystems, Tokyo, Japan). These primers were capable of amplifying human, but not mouse, genes. PCR products were monitored during amplification. All data were calculated by the comparative threshold cycle (Ct) method (22). Occupancy rates of h-hepatocytes in h-hepatocyte regions ranged from 70–95% (Table 2). Contamination of m-hepatocytes did not affect RT-PCR results of human gene expression because each gene's expression level was normalized against h-*GAPDH*.

Responsiveness of h-hepatocytes$_{\text{chimeric mouse}}$ to h-GH and h-IGF-I

Hepatocytes synthesize and secrete IGF-I when GH receptors are activated by GH (23). To determine whether h-GH directly regulates GH-responsive genes or h-IGF-I, h-hepatocytes$_{6YF}$ (9×10^5 cells) from three chimeric mice were cultured in 1.8-cm Matrigel-coated dishes in DMEM as previously reported (24), and 4 h later, they were exposed with 0, 5, and 50 ng/ml h-GH or 50 and 500 ng/ml h-IGF-I for an additional 24 and 48 h and harvested in RLT buffer to prepare total RNA for real-time qRT-PCR.

Gene enrichment analysis

Gene and gene ontology (GO) information were collected from NCBI build 37.1 (ftp://ftp.ncbi.nlm.nih.gov/gene/DATA/gene2go.gz) and The Gene Ontology (http://www.geneontology.org/ontology/gene_ontology.obo) sites, respectively. Pathway information was collected from KEGG (ftp://ftp.genome.jp/pub/kegg/pathway/organisms/hsa/hsa_gene_map.tab) and Ingenuity Pathways Analysis (IPA) software (Ingenuity Systems, Redwood City, CA). The gene enrichment analysis was performed using only GO and pathway groups where at least two genes or more were assigned.

Statistics

Microarray data were evaluated by the Welch's t test (two-sided). The gene enrichment analysis was calculated using Fisher's exact test and corrected with Benjamini-Hochberg's false discovery rate (25). The significance of overlap between two groups of transcripts was determined using Fisher's exact test. Log_{10}-transformed data obtained in real-time qRT-PCR analysis of *in vivo* and *in vitro* studies were analyzed among groups by ANOVA. When the overall F statistics were significant, significance was determined by the Scheffé's test with significance level $\alpha = 0.05$.

Results

Lipid accumulation in chimeric mouse livers

Hepatocytes$_{6YF}$ were transplanted to uPA/SCID mice, and the process of h-hepatocyte repopulation in host livers was visualized using hematoxylin- and eosin-stained histological sections. Vacuoles appeared in the cytoplasm of donor h-hepatocytes approximately 70 d after transplantation and gradually increased in numbers and sizes thereafter (Fig. 1A, a and b). To test whether these vacuoles represent lipid deposits, 36 chimeric mice$_{6YF}$ were killed 48–111 d after transplantation (five before 60 d, 28 between 70 and 90 d, and three after 90 d) for ORO staining of liver sections (Fig. 1B). Most of the chimeric liver h-hepatocytes became ORO$^+$ approximately 70 d after transplantation. The steatosis level was quantified by the size and frequency of ORO$^+$ lipid droplets from grade 0 (Fig. 1Ba) to grade 3 (Fig. 1Bd) and plotted against post-transplantation days (Fig. 1C). Among five livers before 60 d of transplantation, one and four livers were of grade 0 and 1, respectively (Fig. 1C). Most of the livers between 70 and 90 d were of grade 1 (11 of 28 mice) and grade 2

(nine of 28). All three livers after 90 d were of grade 3, showing a good correlation of the steatosis level with post-transplantation duration (~50–110 d). h-IGF-I serum levels of chimeric mice$_{6YF}$, a measure of h-GH level, were under a detection limit of 9.4 ng/ml (n = 3), which supported our previous study that chimeric mouse h-hepatocytes were h-GH deficient (6). Therefore, we considered h-GH deficiency as an etiological factor in the observed hepatic lipogenesis.

Improvement of liver steatosis in chimeric mice by h-GH

To examine the relationship of steatosis with-GH-deficiency, five chimeric mice$_{6YF}$ at different time points after transplantation were infused with h-GH during the last 2 wk before killing (one mouse was killed at 83 d, three at 84 d, and the remaining one at 89 d) and were used as h-GH-treated chimeric mice. Twenty-eight of 36 chimeric mice$_{6YF}$ that were used in the experiment shown in Fig. 1C and killed 70–90 d after transplantation served as controls. The h-IGF-I serum level rose to 72.5 ± 9.4 ng/ml (n = 3) in h-GH-treated mice, a level comparable to that in normal human sera, proving the effectiveness of the h-GH treatment. Serial histological sections were immunostained for h-CK8/18 to identify h-hepatocytes (Fig. 2, A and B) and stained with ORO (Fig. 2, C and D). ORO$^+$ droplets were present in the control mouse h-hepatocytes (Fig. 2, A and C) but were not in h-GH-treated ones (Fig. 2, B and D). Some host m-hepatocytes also contained small cytoplasmic ORO$^+$ droplets (Fig. 2, A and C), probably due to uPA damage because even after h-GH treatment, these lipid droplets remained (Fig. 2, B and D). Steatosis grading on liver sections showed that most of the control mouse livers (93%) were of grade 1–3: 39, 32, and 21% for grades 1, 2, and 3, respectively (Fig. 2E). All h-GH-treated livers were of grade 0. Therefore, we concluded that h-GH plays a critical role in the etiology of human liver steatosis.

h-GH-induced changes in gene expression profiles at the hepatocyte level

Hepatocytes were isolated from three h-GH-untreated chimeric mice$_{9MM}$ 72–101 d after transplantation (nos. 1–3) and three h-GH-treated chimeric mice$_{9MM}$ 75 d after transplantation (nos. 4–6) for microarray analysis (Table 2). We found 15,826 positive transcripts (29%) in 54,675 spotted transcripts in either h-GH-untreated or -treated h-hepatocytes$_{\text{chimeric liver}}$. Among these, 229 (1.4%) and 269 (1.7%) transcripts showed more than 2-fold higher and lower expression levels in h-GH-treated than -untreated h-hepatocytes, respectively. Statistical evaluation at $P < 0.05$ selected 58 genes (82 transcripts) from 229 transcripts as up-regulated in h-GH-treated h-hepatocytes$_{\text{chimeric mouse}}$. Similarly, 33 genes (37 transcripts) were selected from the 269 transcripts as down-regulated genes.

Gene enrichment analysis on transcripts showing more than 2-fold changes selected the significantly overrepresented (GH-induced and -suppressed) GO terms and pathways including GH signaling, IGF-I receptor binding, response to hormone stimulus, lipid biosynthetic process, and aging (Table 4 and Supplemental Table 1, published on The Endocrine Society's Journals Online web site at http://endo.endojournals.org).

TABLE 4. Extracted significantly overrepresented GO terms and pathways

Pathway, or GO term	*P* value	B-H FDR q-value
Hepatocyte level		
Pathway		
GH signaling	0.000244	0.00830
GO molecular function		
IGF receptor binding	3.77×10^{-5}	0.00464
GO biological process		
Response to hormone stimulus	4.30×10^{-5}	0.00556
Lipid biosynthetic process	0.000898	0.0251
Lipid metabolic process	0.00122	0.0284
Aging	0.00288	0.0334
Regulation of fatty acid biosynthetic process	0.00353	0.0358
Regulation of lipid metabolic process	0.0241	0.0947
Tissue level		
Pathway		
Biosynthesis of unsaturated fatty acids	2.78×10^{-5}	0.000584
GH signaling	0.0116	0.0612
GO molecular function		
Stearoyl-coenzyme A 9-desaturase activity	8.78×10^{-5}	0.00382
IGF receptor binding	0.00256	0.0500
GO biological process		
Fatty acid metabolic process	0.000189	0.00585
Lipid metabolic process	0.000739	0.0133
Oxidation reduction	0.00312	0.0288
Response to hormone stimulus	0.00468	0.0346
Aging	0.00627	0.0392
Unsaturated fatty acid biosynthetic process	0.0186	0.0692

B-H FDR, Benjamini-Hochberg's false discovery rate.

h-GH-induced changes in gene expression profiles at the liver tissue level

Identical microarray analysis was performed at the liver tissue level with six chimeric mice$_{6YF}$ (Table 2), with half (nos. 1–3) being used as controls and the other half (nos. 4–6) as h-GH-treated mice. In this analysis, h-hepatocyte-repopulated regions were dissected from liver tissues of these animals and used as h-liver$_{\text{chimeric mouse}}$ as RNA sources for microarray analysis in which 54,675 transcripts were spotted as in the case of the hepatocyte-level analysis. Transcripts positive for either h-GH-untreated or -treated h-liver$_{\text{chimeric mouse}}$ were 18,210 (33%) transcripts, among which 146 (0.8%) and 237 (1.3%) transcripts were expressed at more than 2-fold higher and lower levels, respectively, in h-GH-treated tissues than in h-GH-untreated controls. Through statistical evaluation ($P < 0.05$), we identified 43 genes (64 transcripts) and 55 genes (76 transcripts) as up- and down-regulated genes by h-GH from the 146 and 237 transcripts, respectively.

Gene enrichment analysis on transcripts showing more than 2-fold changes selected the significantly overrepresented (GH-induced and -suppressed) GO terms and pathways including biosynthesis of unsaturated fatty acids, GH signaling, stearoyl-coenzyme A desaturase (SCD) activity, IGF receptor binding, oxidoreductase activity, fatty acid metabolic process, aging were significantly changed (Table 4 and Supplemental Table 2).

In summary, we selected 58 up-regulated and 33 down-regulated genes from the h-hepatocyte-level assay and 43 up-regulated and 55 down-regulated genes from the h-liver tissue-level assay. From them, we chose genes that were commonly up- and down-regulated at both the hepatocyte and liver tissue levels. As a result, 14 up-regulated genes (23 transcripts) and four down-regulated genes (five transcripts) were finally identified as more reliable candidates for h-GH-responsive genes as listed in Table 5, in which the expression ratios at the hepatocyte level [h-GH-treated h-hepatocytes$_{\text{chimeric mouse}}$ *vs.* h-GH-untreated h-

TABLE 5. h-GH-regulated genes

Affymetrix ID	Gene symbol	Accession Number	Gene name	Cell level, treated/untreated		Tissue level, treated/untreated	
				Microarray	RT-PCR[a]	Microarray	RT-PCR[a]
Up-regulated							
209988_s_at	*ASCL1*	NM_004316.3	Achaete-scute complex-like 1	123.39	–	151.42	–
209540_at	*IGF1*[b]	AU144912	IGF-I	179.66	159.83	34.19	35.45
203373_at	*SOCS2*[b]	NM_003877	Suppressor of cytokine signaling 2	39.01	73.79	13.91	53.20
202237_at	*NNMT*[b]	NM_006169	Nicotinamide *N*-methyltransferase	46.02	40.09	14.28	20.79
205978_at	*KL*[b]	NM_004795	Klotho	39.90	22.50	6.58	8.45
207543_s_at	*P4HA1*[b]	NM_000917	Procollagen-proline, 2-oxoglutarate 4-dioxygenase, α-polypeptide I	15.17	11.99	9.69	9.03
203498_at	*DSCR1L1*	NM_005822	Down syndrome critical region gene 1-like 1	5.77	–	4.06	–
215712_s_at	*IGFALS*[b]	AW338791	IGF-binding protein, acid labile subunit	5.29	9.49	7.29	13.63
209967_s_at	*CREM*	D14826	cAMP-responsive element modulator	4.41	–	2.76	–
207256_at	*MBL2*	NM_000242	Mannose-binding lectin 2, soluble	3.44	–	2.09	–
222108_at	*AMIGO2*	AC004010	Adhesion molecule with Ig-like domain 2	2.89	–	2.84	–
201309_x_at	*C5orf13*	U36189	Chromosome 5 open reading frame 13	2.75	–	3.47	–
202234_s_at	*SLC16A1*[b]	BF511091	Solute carrier family 16, member 1	2.74	2.29	4.14	3.84
211056_s_at	*SRD5A1*[b]	BC006373	Steroid-5-α-reductase, α-polypeptide 1	2.29	1.99	2.03	1.72
Down-regulated							
208964_s_at	*FADS1*[b]	AL512760	Fatty acid desaturase 1	0.43	0.51	0.36	0.29
219295_s_at	*PCOLCE2*	NM_013363	Procollagen C-endopeptidase enhancer 2	0.37	–	0.45	–
206561_s_at	*AKR1B10*[b]	NM_020299	Aldo-keto reductase family 1, member B10	0.22	0.22	0.19	0.13
202628_s_at	*SERPINE1*	NM_000602	Serine proteinase inhibitor, clade E, member 1	0.17	–	0.28	–

Treated indicates h-GH-treated chimeric mouse, whereas untreated indicates h-GH-untreated chimeric mouse. –, Not determined.

[a] The expression level of each gene was divided with that of h-*GAPDH*.

[b] Gene expression levels were determined by both microarray assay and real-time qRT-PCR.

hepatocytes$_{\text{chimeric mouse}}$ (cell level, treated/untreated)] and at the tissue level [h-GH-treated h-liver$_{\text{chimeric mouse}}$ *vs.* -untreated h-liver$_{\text{chimeric mouse}}$ (tissue level, treated/untreated)] are presented for each gene. *P* values for overrepresentation of the overlapping genes (up- and down-regulated genes in both hepatocytes and liver tissue levels) were 5.34×10^{-9} and 1.92×10^{-9}, respectively, which indicates the significance of the overlapping.

The microarray assay's results were validated by real-time qRT-PCR using RNA extracted from the sources shown in Table 2 on arbitrarily selected eight and three genes from the above final 14 h-GH-up- and four h-GH-down-regulated genes, respectively: *IGF-I*, suppressor of cytokine signaling 2 (*SOCS2*), nicotinamide *N*-methyltransferase (*NNMT*), *KL*, *P4HA1*, *IGFALS*, solute carrier family 16/member 1 (*SLC16A1*), and steroid-5-α-reductase and α-polypeptide 1 (*SRD5A1*) as h-GH-up-regulated genes and fatty acid desaturase (*FADS1*) and aldo-keto reductase family 1/member B10 (*AKR1B10*) as h-GH-down-regulated genes. The expression ratios (treated/untreated) calculated from the qRT-PCR results are included in Table 5, which well support the microarray data, indicating the reliability of the microarray data.

There was the possibility that mouse transcripts were also included as the cDNAs hybridized in the currently adopted microarray assay. To check this possibility, pooled cDNAs of three uPA/SCID mouse livers were subjected to the microarray with 54,675 cDNA spots, which gave a result that 5,643 of 54,675 transcripts (10.3%) were positive. Sixteen genes among the genes listed in Table 5 were not found in these positive genes, but two genes, *SOCS2* and *IGFALS*, both h-GH-up-regulated genes, were found there. Considering that the cross-hybridized signals were less than 10% of those in the GH-untreated hepatocytes$_{\text{chimeric mouse}}$ and the contamination of mouse hepatocytes in the h-hepatocyte preparation used in the present study was less than 10% (Table 2, 9MM nos. 1–6), we concluded that their ratios of treated to untreated genes were high enough to include them as h-GH-regulated genes in the present study. This conclusion was further validated by measuring m-Alb mRNA expression levels in the h-liver$_{\text{chimeric mouse}}$. Real-time qRT-PCR was performed for RNAs isolated from h-liver$_{\text{chimeric mouse}}$ (Table 2, 6YF nos. 1–6) using a set of m-Alb primers. The result showed that m-Alb expression levels in the h-liver$_{\text{chimeric mouse}}$ were 0.5 ± 0.2% of those of the uPA/SCID mouse liver. As a whole, it can be said that the cross-reactivity does not affect the results in the present study.

Improvement of gene expression by h-GH

Real-time qRT-PCR was performed for livers of h-GH-untreated chimeric, h-GH-treated chimeric mice, and humans, the last of which accurately reflect the physiology of h-GH endocrine regulation. The h-GH-untreated and -treated h-hepatocytes$_{\text{chimeric mouse}}$ were isolated from nos. 1–3 and nos. 4–6 of chimeric mice$_{\text{9MM}}$, respectively (Table 2). The h-GH-untreated and -treated h-liver$_{\text{chimeric mouse}}$ were isolated from nos. 1–3 and nos. 4–6 of chimeric mice$_{\text{6YF}}$, respectively (Table 2). The h-hepatocytes$_{\text{human}}$ and h-liver$_{\text{human}}$ were isolated from four (28YM, 57YM, 25YF, and 61YF) and three (28YM, 25YF, and 61YF) donors, respectively (Table 1). Expression levels in h-hepatocytes$_{\text{chimeric mouse}}$ and h-liver$_{\text{chimeric mouse}}$ under h-GH-untreated and -treated conditions were divided by the h-hepatocyte$_{\text{human}}$ and the h-liver$_{\text{human}}$, respectively, which is shown as the hepatocyte ratio (*white bars*) and liver-tissue ratio (*black bars*), respectively (Fig. 3). The ratios are used as measures of the extent of difference/closeness of the gene expression level in h-GH-treated or -untreated chimeric livers from/to that in human liver. If h-GH improves gene expressions in chimeric mouse livers, ratios for h-GH-up-regulated genes in h-GH-untreated and -treated chimeric liver are expected to be less than 1 and approximately 1, respectively, and ratios for h-GH-down-regulated genes in h-GH-untreated and -treated chimeric liver are expected to be more than 1 and approximately 1, respectively.

Expression levels of a total of eight h-GH-up-regulated genes were compared between h-GH-untreated and -treated chimeric mice at both hepatocyte and liver tissue levels. The results of the h-GH-up-regulated genes are shown in Fig. 3A. Generally, the expressions of the genes, except *KL*, were significantly suppressed in the absence of h-GH at both the hepatocyte and liver tissue levels. Expression in h-GH-treated cases was similar to that in human livers: *IGF-I* and *P4AH1* at the tissue level and *IGFALS* and *SLC16A1* at both levels. *KL* expression in h-GH-untreated chimeric mice was similar to that in human livers at both levels, and h-GH treatment markedly increased expression over that in human livers at both levels, suggesting that its expression is greatly up-regulated by GH. *In vivo*, h-GH-up-regulated genes of human livers are likely positively induced by GH.

Our results on suppression of spontaneous lipogenesis by GH (Fig. 2) and a reported relationship between GH-responsive genes and lipogenesis-related genes (26) suggest an association between the h-GH-responsive genes listed in Table 5 and the observed hepatic lipogenesis. Gene enrichment analysis showed that h-GH-responsive genes were enriched as those involved in the lipid synthesis process, lipid metabolic process, and regulation of fatty acid biosynthetic process (Table 4). Of the two down-regulated genes, *FADS1* is known to be lipogenesis related (27), and *AKR1B10* was recently reported to regulate fatty acid synthesis (28). Five genes were additionally cho-

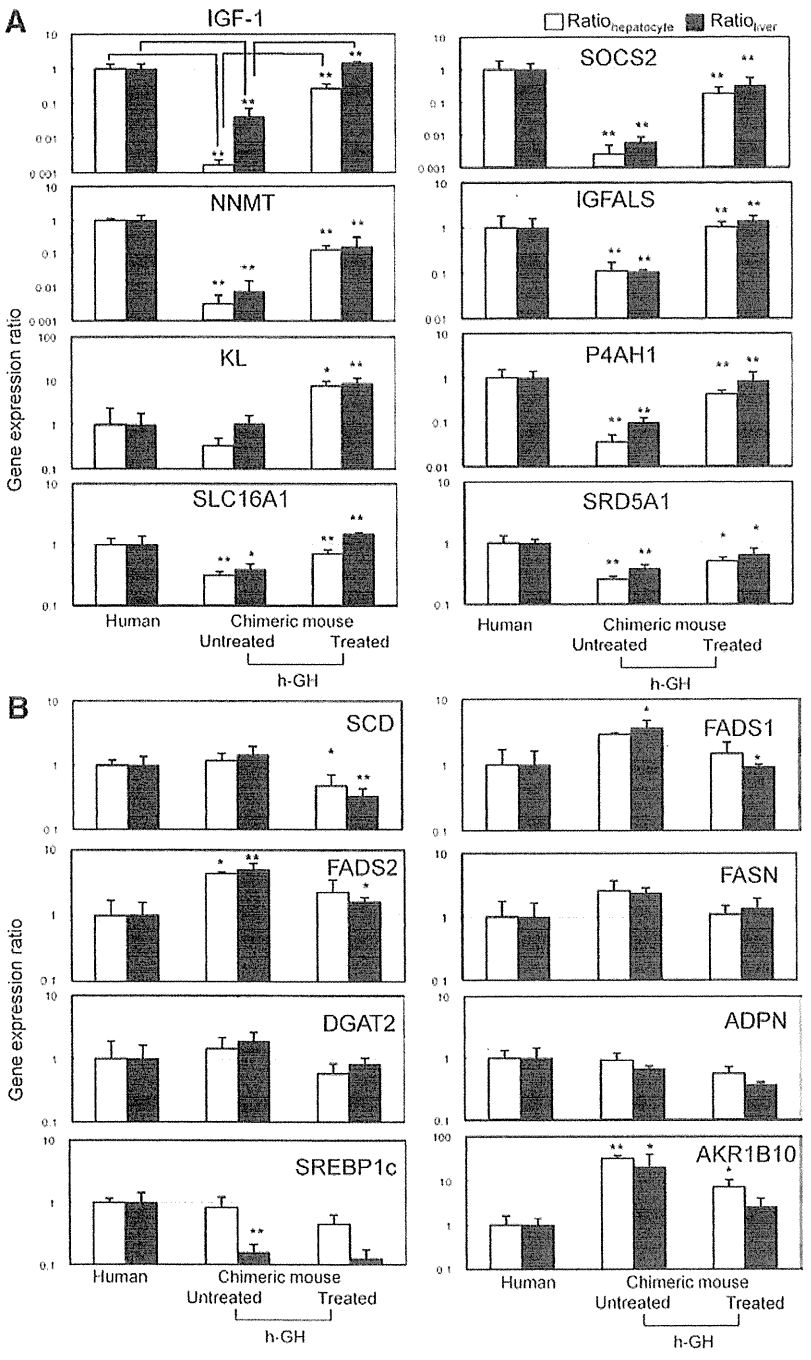

FIG. 3. Regulation of gene expression in h-hepatocytes$_{\text{chimeric mouse}}$ by h-GH at the hepatocyte and liver tissue levels. Six chimeric mice$_{9MM}$ and six chimeric mice$_{6YF}$ were produced (Table 2); half of each group (nos. 1–3 for both the chimeric mice$_{9MM}$ and chimeric mice$_{6YF}$) served as control animals, and the remaining half (nos. 4–6 for both the chimeric mice$_{9MM}$ and chimeric mice$_{6YF}$) were treated with h-GH. h-Hepatocytes$_{\text{chimeric mouse}}$ and h-livers$_{\text{chimeric mouse}}$ were isolated from the former and latter chimeric mice, respectively. h-Hepatocytes$_{\text{human}}$ and h-livers$_{\text{human}}$ were also isolated from four (25YF, 28YM, 57YM, and 61YF) and three (25YF, 28YM and 61YF) human donors, respectively (Table 1). RNA was isolated from the hepatocytes and liver tissue for real-time qRT-PCR analysis. qRT-PCR was performed for eight h-GH-up-regulated (A) and eight lipogenesis-related (B) genes. The expression level of each gene was normalized against that of h-*GAPDH*. The expression level of h-GH-untreated h-hepatocytes$_{\text{chimeric mouse}}$ and h-GH-treated h-hepatocytes$_{\text{chimeric mouse}}$ was divided by that of h-hepatocytes$_{\text{human}}$ (ratio$_{\text{hepatocyte}}$). Similarly, the expression level of h-livers$_{\text{chimeric mouse}}$ was divided by that of h-livers$_{\text{human}}$ (ratio$_{\text{liver}}$). *White* and *black bars* represent the ratio$_{\text{hepatocyte}}$ and the ratio$_{\text{liver}}$, respectively. Each value represents the mean ± SD. *Asterisks above bars* of untreated chimeric mouse show significance between human and GH-untreated chimeric mouse. *Asterisks above bars* of treated chimeric mouse show significance between human and GH-treated chimeric mouse. *, $P < 0.05$; **, $P < 0.01$.

sen to examine the relationship between h-GH-down-regulated genes and known lipogenic genes from previous studies: *FADS2* (27), *SCD* (29), *FASN* (30), diacylglycerol acyltransferase 2 gene (*DGAT2*) (31), and the adiponutrin gene [*ADPN* (32), currently known as *PNPLA3* (33)]. These genes were included as h-GH-down-regulated genes at either the hepatocyte or liver tissue level in the microarray assay; *FADS2* and *SCD* were significantly ($P < 0.05$) down-regulated only at the liver tissue level, *FASN* was insignificantly (>2-fold) down-regulated only at the hepatocyte level, *DGAT2* was insignificantly (>2-fold) down-regulated only at the hepatocyte level, and *ADPN* significantly ($P < 0.05$) decreased its expression only at the hepatocyte level. Two known GH-inducible lipogenesis-related genes, *SREBP1c* (34–36) and fatty acid-binding protein gene (*FABP*) (24, 37), were also chosen from previous studies.

Expression of a total of nine genes was compared between human livers and h-GH-untreated and -treated chimeric mice at both hepatocyte and liver tissue levels as above. Results for lipogenesis-related genes are shown in Fig. 3B. Ratios of three genes, *FADS1* (significant at tissue level), *FADS2* (significant at both levels), and *AKR1B10* (significant at both levels), were higher in the h-GH-untreated chimeric mice compared with humans, and h-GH treatment lowered the ratios of *SCD* (significant at both levels), *FADS1* (significant at tissue level), *FADS2* (significant at tissue level), and *AKR1B10* (significant at hepatocyte level). Although not significantly, ratios of *FASN* and *DGAT2* were also higher in the h-GH-untreated chimeric mice compared with humans and decreased by h-GH treatment. *ADPN* expression in h-GH-untreated chimeric mice was close to that in humans at both levels, and h-GH treatment decreased ratios (insignificant). Thus, it is most likely that these lipogenesis-related genes are down-regulated by h-GH. Ratios of *SREBP1c* (Fig.

3B) and *FABP* (data not shown) genes did not show any meaningful changes by h-GH at either the hepatocyte or liver tissue level under the observed endocrinological conditions, although *SREBP1* expression was significantly lower at tissue levels in h-GH-untreated chimeric mice compared with human.

Deletion of GH receptor gene (*GHR*) in mice resulted in an increase of insulin receptor gene (*IRS*) expression (38) and a reduction of plasma levels of IGF-I, insulin, and glucose, implying that the mice increased insulin sensitivity (39, 40). These studies suggested the possibility that chimeric mice are insulin sensitive. Thus, we examined whether chimeric mice are insulin sensitive by determining the expression levels of h-*GHR* and h-*IRS*. Real-time qRT-PCR analysis showed that h-*GHR* and h-*IRS* expression levels in chimeric mice were similar or higher than humans, and h-GH administration of chimeric mice did not affect these observed expression levels. However chimeric mice did not show any sign of insulin resistance or sensitivity in a sugar tolerance test (data not shown). As a whole, we currently consider that chimeric mice are not insulin sensitive.

In vitro effects of h-GH on gene expressions in h-hepatocytes

We asked whether the aforementioned effects of h-GH on the h-GH-up-regulated gene and lipogenic gene expression in chimeric mouse livers *in vivo* are reproducible *in vitro*. h-Hepatocytes$_{6YF}$ isolated from three chimeric mice with RI_{Alb} higher than 95% at 70–80 d after transplantation were cultured for 24 and 48 h in the presence and absence of h-GH and h-IGF-I, followed by determination of expression levels of the eight h-GH-up-regulated genes by real-time qRT-PCR (Fig. 4A). Expression of *IGF-I*, *SOCS2*, *NNMT*, *IGFALS*, and *P4AH1* were significantly increased by h-GH in a dose-dependent manner, but h-IGF-I did not enhance expression of the genes, indicating the direct the action of h-GH on the expression of these genes. The remaining three genes (*KL*, *SLC16A1*, and *SRD5A1*) were not responsive to h-GH or h-IGF-I.

Results for lipogenic genes (*SCD*, *FADS1*, *FADS2*, *FASN*, *DGAT2*, *ADPN*, *AKR1B10*, and *SREBP1c*) are shown in Fig. 4B. Only *FADS1*, *DGAT2*, *SREBP1c*, and *AKR1B10* significantly decreased the expression at 24 or 48 h exposure of 50 ng/ml h-GH. Although insignificant, *SCD*, *FADS2*, and *FASN* were decreased by GH exposure. The expression levels of the eight genes did not significantly change by h-IGF-I.

Discussion

GH regulation of lipogenic genes has been generally studied using rodents (34–37, 41–43), and no suitable animal model whose liver mimics the human liver has been available. Currently, we propose an h-hepatocyte-bearing chimeric mouse as one such model, in which heavy lipid accumulation spontaneously takes place in h-hepatocytes more than 2 months after transplantation but does not when the animals are administered h-GH. Using this model, we demonstrated that h-GH deficiency is a cause of the steatosis and identified 14 and four genes as h-GH-up- and -down-regulated genes at both the hepatocyte and liver tissue level, in which three new lipogenic genes (*FADS1*, *FADS2*, and *AKR1B10*) were included. Regarding h-GH-down-regulated genes, we characterized an additional seven lipogenic genes, although these genes were h-GH down-regulated only at the hepatocyte level or liver tissue level. *FADS1*, *FADS2*, and *AKR1B10* were included in these seven genes and were significantly up-regulated in the chimeric mouse liver compared with human liver, but their expression was down-regulated by h-GH. Thus, it is suggested that these genes participate in the spontaneous steatosis observed in the chimeric mouse liver.

Results of previous studies indicated the presence of species differences in GH responsiveness of lipogenic genes between rats and mice. *SREBP-1c*, a known transcription factor of lipogenic genes, and its target genes, *FASN* and *SCD-1*, appear to be GH up-regulated in rats; hypophysectomy decreases expression of these genes, and the infusion of the rats with GH improved their expression to the original levels (34, 35). By contrast, a study with GH-transgenic technology showed that the same genes were down-regulated in mice (44). Recent microarray analysis supported such species differences; GH treatment suppressed *SCD* gene expression level in hypophysectomized mouse livers (42) but not in hypophysectomized rat livers (41). There are also differences regarding GH responsiveness of lipogenic genes between *in vitro* and *in vivo* studies; the above cited authors showed in a study with primary cultures of rat hepatocytes *SCD1* as GH up-regulated, *FASN* as GH down-regulated, and *SREBP-1c* as GH non-responsive (34). In the present study, expression of h-*SCD*, but not h-*SREBP-1c*, was reduced by h-GH administration to the chimeric mice, and h-*FABP* expression was not affected by h-GH, which was different from a rat study (34). h-*FADS1*, h-*FADS2*, and h-*AKR1B10* were down-regulated in the present study, but they did not report them as GH-down-regulated genes in rodent studies. In addition, AGHD patients show fatty liver and nonalcoholic steatohepatitis (NASH) (8), and GH treatment improved the symptoms (13, 14). However, studies using hypophysectomized rodents did not report such changes (34, 35, 41, 42).

The serum concentration of GH is low in nonalcoholic fatty liver disease (NAFLD) patients (15), and *NNMT* and

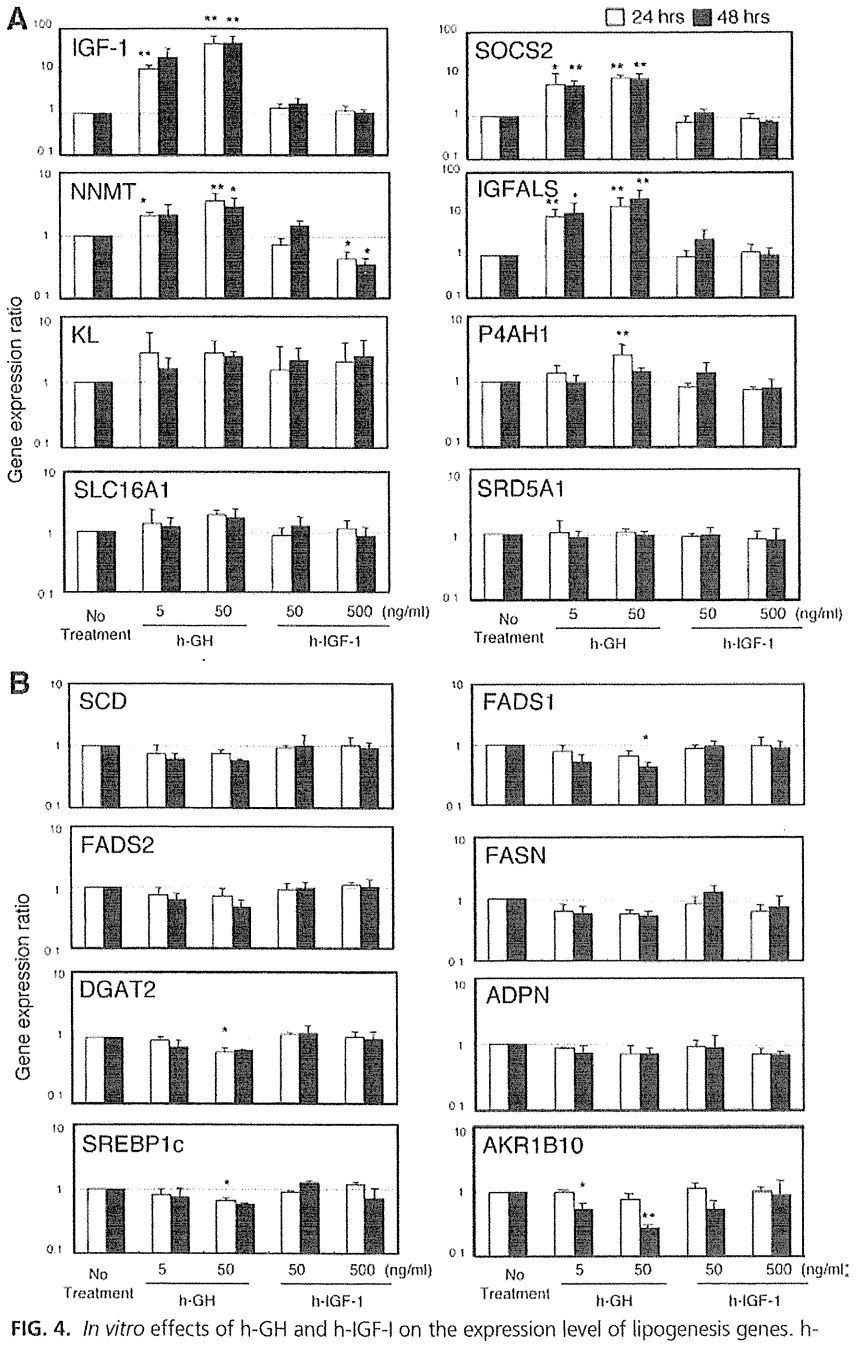

FIG. 4. *In vitro* effects of h-GH and h-IGF-I on the expression level of lipogenesis genes. h-Hepatocytes$_{6YF}$ were cultured with 0, 5, or 50 ng/ml h-GH or 50 or 500 ng/ml h-IGF-I for 24 and 48 h and subjected to RNA isolation to perform real-time qRT-PCR analysis for eight h-GH-up-regulated genes (A) and eight lipogenesis-related genes (B). The expression level of each gene was normalized against that of h-*GAPDH*. The gene expression level of h-hepatocytes treated with h-GH or h-IGF-I was divided by that of untreated h-hepatocytes. *White* and *black bars* represent 24 and 48 h, respectively. Each value represents the mean ± SD. *Asterisks above a bar* show significance between no treatment and each dose of h-GH or h-IGF-I treatment. *, $P < 0.05$; **, $P < 0.01$.

IGFALS are up-regulated in NASH patients (47). Fatty livers of chimeric mice in the present study appreciably reproduce expression profiles of these known NAFLD/NASH-associated genes. We showed that h-GH regulates h-*SCD* and other lipogenesis-related genes, including h-*FADS1*, h-*FADS2*, and h-*AKR1B10* in a h-*SREBP1*-independent manner. Thus, chimeric mice could be particularly useful as an NAFLD/NASH mouse model, with the genes identified in this study serving as therapeutic target genes for NAFLD patients.

Among 14 h-GH-up-regulated genes characterized in this study, eight genes (*IGF-I*, *SOCS2*, *NNMT*, *P4HA1*, *IGFALS*, *MBL2 AMIGO2*, and *SRD5A1*) are known GH-up-regulated genes (23, 41–43, 45), but the remaining six h-GH-up-regulated genes (*ASCL1*, *KL*, *DSCR1L1*, *CREM*, *C5orf13*, and *SLC16A1*) have never been reported as up-regulated genes. Roles of these newly identified GH-up-regulated genes in the human liver could be further investigated using the chimeric mice.

The protein Klotho is known to inhibit insulin/IGF-I signaling, which likely increases resistance to oxidative stress and potentially contributes to its claimed anti-aging properties (46). In the present study, *KL* expression levels were similar in human and chimeric mouse livers, but h-GH markedly induced *KL* gene expression in the latter. The findings of the present study suggested a mutual regulatory mechanism(s) between the two genes: *h-GH* might play a role in the anti-aging process through the *KL* induction.

We were able to propagate h-hepatocytes in chimeric mouse livers, which could solve the problem of a quite limited availability of human hepatocytes for research purposes. In fact, in the present study, we showed the usefulness of chimeric mouse-derived h-hepatocytes for *in vitro* study by testing the effects of h-GH or h-IGF-I on expression levels of eight lipogenic genes that had been up-regulated in chimeric mouse liver *in vivo*. We were able to answer a question of whether h-GH and h-IGF-I in combination directly or indirectly induce such changes in gene expression. Hepatocytes in conventional two-dimensional culture do not generally recapitulate gene expression profiles observed under *in vivo* conditions. In the present study, hepatocytes were three-

dimensionally cultured on Matrigel (spheroid culture), which allowed them to express gene expression closer to *in vivo* conditions as reported previously (48).

We resected h-hepatocyte regions from chimeric livers for microarray analysis and real-time RT-PCR. The gene expression profiles determined using the dissected regions were similar to those determined using the isolated h-hepatocytes$_{\text{chimeric mouse}}$. This finding also indicates the usability of chimeric mouse liver tissues as an alternative RNA source to h-hepatocytes, whose isolation is time consuming and laborious.

In conclusion, the present study shows that chimeric mice could overcome the species difference between experimental animals and humans, and therefore, these mice are useful for investigating the mechanism of the action of GH on h-hepatocytes *in vivo* and role of GH in NAFLD/NASH.

Acknowledgments

We thank Y. Yoshizane, H. Kohno, Y. Matsumoto, and S. Nagai for their technical assistance.

Address all correspondence and requests for reprints to: Katsutoshi Yoshizato, Ph.D., or Chise Tateno, Ph.D., PhoenixBio. Co. Ltd., 3-4-1 Kagamiyama, Higashihiroshima, Hiroshima 739-0046, Japan. E-mail: katsutoshi.yoshizato@phoenixbio.co.jp or chise.mukaidani@phoenixbio.co.jp.

This work was supported by the Yoshizato Project, Cooperative Link of Unique Science and Technology for Economy Revitalization (CLUSTER), Japan.

Disclosure Summary: The authors have no conflicts of interest to disclose.

References

1. Tateno C, Yoshizane Y, Saito N, Kataoka M, Utoh R, Yamasaki C, Tachibana A, Soeno Y, Asahina K, Hino H, Asahara T, Yokoi T, Furukawa T, Yoshizato K 2004 Near-completely humanized liver in mice shows human-type metabolic responses to drugs. Am J Pathol 165:901–912
2. Yoshizato K, Tateno C 2009 A human hepatocyte-bearing mouse: an animal model to predict drug metabolism and effectiveness in humans. PPAR Res 2009:476217
3. Yoshizato K, Tateno C 2009 In vivo modeling of human liver for pharmacological study using humanized mouse. Expert Opin Drug Metab Toxicol 5:1435–1446
4. Katoh M, Matsui T, Okumura H, Nakajima M, Nishimura M, Naito S, Tateno C, Yoshizato K, Yokoi T 2005 Expression of human phase II enzymes in chimeric mice with humanized liver. Drug Metab Dispos 33:1333–1340
5. Nishimura M, Yoshitsugu H, Yokoi T, Tateno C, Kataoka M, Horie T, Yoshizato K, Naito S 2005 Evaluation of mRNA expression of human drug-metabolizing enzymes and transporters in chimeric mouse with humanized liver. Xenobiotica 35:877–890
6. Masumoto N, Tateno C, Tachibana A, Utoh R, Morikawa Y, Shimada T, Momisako H, Itamoto T, Asahara T, Yoshizato K 2007 GH enhances proliferation of human hepatocytes grafted into immunodeficient mice with damaged liver. J Endocrinol 194:529–537
7. Souza SC, Frick GP, Wang X, Kopchick JJ, Lobo RB, Goodman HM 1995 A single arginine residue determines species specificity of the human growth hormone receptor. Proc Natl Acad Sci USA 92:959–963
8. Brunt EM 2010 Pathology of nonalcoholic fatty liver disease. Nat Rev Gastroenterol Hepatol 7:195–203
9. Johannsson G, Bengtsson BA 1999 Growth hormone and the metabolic syndrome. J Endocrinol Invest 22:41–46
10. Ichikawa T, Nakao K, Hamasaki K, Furukawa R, Tsuruta S, Ueda Y, Taura N, Shibata H, Fujimoto M, Toriyama K, Eguchi K 2007 Role of growth hormone, insulin-like growth factor 1 and insulin-like growth factor-binding protein 3 in development of non-alcoholic fatty liver disease. Hepatol Int 1:287–294
11. Ichikawa T, Hamasaki K, Ishikawa H, Ejima E, Eguchi K 2003 Non-alcoholic steatohepatitis and hepatic steatosis in patients with adult onset growth hormone deficiency. Gut 52:914
12. Adams LA, Feldstein A, Lindor KD, Angulo P 2004 Nonalcoholic fatty liver disease among patients with hypothalamic and pituitary dysfunction. Hepatology 39:909–914
13. Takahashi Y, Iida K, Takahashi K, Yoshioka S, Fukuoka H, Takeno R, Imanaka M, Nishizawa H, Takahashi M, Seo Y, Hayashi Y, Kondo T, Okimura Y, Kaji H, Kitazawa R, Kitazawa S, Chihara K 2007 Growth hormone reverses nonalcoholic steaotohepatitis in patients with adult growth hormone deficiency. Gastroenterology 132:938–943
14. Lonardo A, Carani C, Carulli N, Loria P 2006 'Endocrine NAFLD' a hormonocentric perspective of nonalcoholic fatty liver disease pathogenesis. J Hepatol 44:1196–1207
15. Lonardo A, Loria P, Leonardi F, Ganazzi D, Carulli N 2002 Growth hormone plasma levels in nonalcoholic fatty liver disease. Am J Gastroenterol 97:1071–1072
16. Meuleman P, Vanlandschoot P, Leroux-Roels G 2003 A simple and rapid method to determine the zygosity of uPA-transgenic SCID mice. Biochem Biophys Res Commun 308:375–378
17. Jeschke MG, Herndon DN, Finnerty CC, Bolder U, Thompson JC, Mueller U, Wolf SE, Przkora R 2005 The effect of growth hormone on gut mucosal homeostasis and cellular mediators after severe trauma. J Surg Res 127:183–189
18. Utoh R, Tateno C, Yamasaki C, Hiraga N, Kataoka M, Shimada T, Chayama K, Yoshizato K 2008 Susceptibility of chimeric mice with livers repopulated by serially subcultured human hepatocytes to hepatitis B virus. Hepatology 47:435–446
19. Utoh R, Tateno C, Kataoka M, Tachibana A, Masumoto N, Yamasaki C, Shimada T, Itamoto T, Asahara T, Yoshizato K 2010 Hepatic hyperplasia associated with discordant xenogeneic parenchymal-nonparenchymal interactions in human hepatocyte-repopulated mice. Am J Pathol 177:654–665
20. Tateno C, Takai-Kajihara K, Yamasaki C, Sato H, Yoshizato K 2000 Heterogeneity of growth potential of adult rat hepatocytes in vitro. Hepatology 31:65–74
21. Igarashi Y, Tateno C, Tanaka Y, Tachibana A, Utoh R, Kataoka M, Ohdan H, Asahara T, Yoshizato K 2008 Engraftment of human hepatocytes in the livers of rats reconstructed with bone marrow cells from an immunodeficient mouse. Xenotransplantation 15:235–245
22. Asahina K, Sato H, Yamasaki C, Kataoka M, Shiokawa M, Katayama S, Tateno C, Yoshizato K 2002 Pleiotrophin/HB-GAM as a mitogen of rat hepatocytes and its role in regeneration and development of liver. Am J Pathol 160:2191–2205
23. Gosteli-Peter MA, Winterhalter KH, Schmid C, Froesch ER, Zapf J 1994 Expression and regulation of insulin-like growth factor (IGF-I) and IGF-binding protein messenger ribonucleic acid levels in tissues and hypophysectomized rats infused with-IGF-I and growth hormone. Endocrinology 135:2558–2567
24. Thissen JP, Pucilowska JB, Underwood LE 1994 Differential reg-

ulation of insulin-like growth factor I (IGF-I) and IGF binding protein-1 messenger ribonucleic acids by amino acid availability and growth hormone in rat hepatocyte primary culture. Endocrinology 134:1570–1576
25. Benjamini Y, Hochberg Y 1995 Controlling the false discovery rate: a practical and powerful approach to multiple testing. J Roy Stat Soc Ser B 57:289–300
26. Ståhlberg N, Merino R, Hernández LH, Fernández-Pérez L, Sandelin A, Engström P, Tollet-Egnell P, Lenhard B, Flores-Morales A 2005 A Exploring hepatic hormone actions using a compilation of gene expression profiles. BMC Physiol 5:8
27. Glaser C, Heinrich J, Koletzko B 2010 Role of FADS1 and FADS2 polymorphisms in polyunsaturated fatty acid metabolism. Metabolism 59:993–999
28. Ma J, Yan R, Zu X, Cheng JM, Rao K, Liao DF, Cao D 2008 Aldo-keto reductase family 1 B10 affects fatty acid synthesis by regulating the stability of acetyl-CoA carboxylase-α in breast cancer cells. J Biol Chem 283:3418–3423
29. Ntambi JM 1992 Dietary regulation of stearoyl-CoA desaturase 1 gene expression in mouse liver. J Biol Chem 267:10925–10930
30. Menendez JA, Lupu R 2007 Fatty acid synthase and the lipogenic phenotype in cancer pathogenesis. Nat Rev Cancer 7:763–777
31. Choi CS, Savage DB, Kulkarni A, Yu XX, Liu ZX, Morino K, Kim S, Distefano A, Samuel VT, Neschen S, Zhang D, Wang A, Zhang XM, Kahn M, Cline GW, Pandey SK, Geisler JG, Bhanot S, Monia BP, Shulman GI 2007 Suppression of diacylglycerol acyltransferase-2 (DGAT2), but not DGAT1, with antisense oligonucleotides reverses diet-induced hepatic steatosis and insulin resistance. J Biol Chem 282:22678–22688
32. Baulande S, Lasnier F, Lucas M, Pairault J 2001 Adiponutrin, a transmembrane protein corresponding to a novel dietary- and obesity-linked mRNA specifically expressed in the adipose lineage. J Biol Chem 276:33336–33344
33. Huang Y, He S, Li JZ, Seo YK, Osborne TF, Cohen JC, Hobbs HH 2010 A feed-forward loop amplifies nutritional regulation of PNPLA3. Proc Natl Acad Sci USA 107:7892–7897
34. Améen C, Lindén D, Larsson BM, Mode A, Holmäng A, Oscarsson J 2004 Effects of gender and GH secretory pattern on sterol regulatory element-binding protein-1c and its target genes in rat liver. Am J Physiol Endocrinol Metab 287:E1039–E1048
35. Frick F, Lindén D, Améen C, Edén S, Mode A, Oscarsson J 2002 Interaction between growth hormone and insulin in the regulation of lipoprotein metabolism in the rat. Am J Physiol Endocrinol Metab 283:E1023–E1031
36. Shimano H, Yahagi N, Amemiya-Kudo M, Hasty AH, Osuga J, Tamura Y, Shionoiri F, Iizuka Y, Ohashi K, Harada K, Gotoda T, Ishibashi S, Yamada N 1999 Sterol regulatory element-binding protein-1 as a key transcription factor for nutritional induction of lipogeneic enzyme genes. J Biol Chem 274:35832–35839
37. Carlsson L, Nilsson I, Oscarsson J 1998 Hormonal regulation of liver fatty acid-binding protein *in vivo* and *in vitro*: effects of growth hormone and insulin. Endocrinology 139:2699–2709
38. Panici JA, Wang F, Bonkowski MS, Spong A, Bartke A, Pawlikowska L, Kwok PY, Masternak MM 2009 Is altered expression of hepatic insulin-related genes in growth hormone receptor knockout mice due to GH resistance or a difference in biological life spans? J Gerontol A Biol Sci Med Sci. 2009 64:1126–1133
39. Liu JL, Coschigano KT, Robertson K, Lipsett M, Guo Y, Kopchick JJ, Kumar U, Liu YL 2004 Disruption of growth hormone receptor gene causes diminished pancreatic islet size and increased insulin sensitivity in mice. Am J Physiol Endocrinol Metab 287:E405–E413
40. Dominici FP, Arostegui Diaz G, Bartke A, Kopchick JJ, Turyn D 2000 Compensatory alterations of insulin signal transduction in liver of growth hormone receptor knockout mice. J Endocrinol 166: 579–590
41. Wauthier V, Waxman DJ 2008 Sex-specific early growth hormone response genes in rat liver. Molecular Endocrinology 22:1962–1974
42. Wauthier V, Sugathan A, Meyer RD, Dombkowski AA, Waxman DJ 2010 Division of cell and molecular biology intrinsic sex differences in the early growth hormone responsiveness of sex-specific genes in mouse liver. Mol Endocrinol 24:667–678
43. Tollet-Egnell P, Flores-Morales A, Stavréus-Evers A, Sahlin L, Norstedt G 1999 Growth hormone regulation of SOCS-2, SOCS-3, and CIS messenger ribonucleic acid expression in the rat. Endocrinology 140:3693–3704
44. Olsson B, Bohlooly-Y M, Brusehed O, Isaksson OG, Ahrén B, Olofsson SO, Oscarsson J, Törnell J 2003 Bovine growth hormone-transgenic mice have major alterations in hepatic expression of metabolic genes. Am J Physiol Endocrinol Metab 285:E504–E511
45. Hansen TK, Thiel S, Dall R, Rosenfalck AM, Trainer P, Flyvbjerg A, Jørgensen JO, Christiansen JS 2001 GH strongly affects serum concentrations of mannan-binding lectin: evidence for a new IGF-I independent immunomodulatory effect of GH. J Clin Endocrinol Metab 86:5383–5388
46. Yamamoto M, Clark JD, Pastor JV, Gurnani P, Nandi A, Kurosu H, Miyoshi M, Ogawa Y, Castrillon DH, Rosenblatt KP, Kuro-o M 2005 Regulation of oxidative stress by the anti-aging hormone klotho. J Biol Chem 280:38029–38034
47. Younossi ZM, Gorreta F, Ong JP, Schlauch K, Del Giacco L, Elariny H, Van Meter A, Younoszai A, Goodman Z, Baranova A, Christensen A, Grant G, Chandhoke V 2005 Hepatic gene expression in patients with obesity-related non-alcoholic steatohepatitis. Liver Int 25:760–771
48. Schuetz EG, Li D, Omiecinski CJ, Muller-Eberhard U, Kleinman HK, Elswick B, Guzelian PS 1988 Regulation of gene expression in adult rat hepatocytes cultured on a basement membrane matrix. J Cell Physiol 134:309–323